Middle to late Holocene decreased fluvial aggradation and widespread peat initiation in the Ishikari lowland (northern Japan)

Yuji Ishii[1,2], Kazuaki Hori[1], Arata Momohara[3], Toshimichi Nakanishi[4] and Wan Hong[5]

[1]Department of Geography, Graduate School of Environmental Studies, Nagoya University, Japan

[2]Research Fellow of the Japan Society for the Promotion of Science

[3]Faculty of Horticulture, Chiba University, Japan

[4]AIG Collaborative Research Institute for International Study on Eruptive History and Informatics, Fukuoka University, Japan

[5]Geochemical Analysis Center, Korean Institute of Geoscience and Mineral Resources (KIGAM), Korea Rep.

Corresponding author: Yuji Ishii, Department of Geography, Graduate School of Environmental Studies, Nagoya University, Furo-cho, Chikusa-ku, Nagoya 464-8601, Japan.

Email: ishii.yuuji@f.mbox.nagoya-u.ac.jp

Abstract

This study investigated the influence of sea-level and climate changes on the decreased fluvial aggradation and subsequent widespread peat initiation in the middle to late Holocene in the Ishikari lowland, which is a coastal floodplain formed in response to the postglacial sea-level change. By introducing a new approach to separately evaluate the rates of organic and clastic sediment input, we demonstrated that the peat began to form when the fluvial sedimentation rate was significantly decreased (less than 0.6 mm/yr), while plant macrofossil analysis suggested that lowering of water level is also important to the peat initiation. Such changes in sedimentary environment may be associated with the abrupt abandonment of crevasse splays. The concentrated ages of the peat initiation around 5600–5000, 4600–4300, and 4100–3600 cal BP suggests that an allogenic control promoted the abandonment of crevasse splays, and different onset ages can be explained by different fluvial responses of the Ishikari River and its tributaries. The abandonment of crevasse splays could result from sea-level fall or decreased precipitation. While submillennial sea-level fluctuations coincident with the peat initiation have not been reported in coastal lowlands of Japan, the close comparison of the onset ages and decreased precipitation recorded in a stalagmite from China, which represents the strength of the East Asian summer monsoon, suggests that decrease in precipitation led to the abandonment of crevasse splays. Our results may indicate that similar fluvial responses might be common in other coastal floodplains affected by the East Asian summer monsoon.

Keywords

coastal floodplain, fluvial aggradation, peat, East Asian summer monsoon, climate change, Holocene

Introduction

The evolution of coastal floodplains in response to sea-level and climate changes, before significant human impact on landscape by agricultural and industrial activities, have received considerable interest within the field of fluvial geomorphology and sedimentology (Blum and Törnqvist, 2000), and they are also relevant to understanding of human activities in the past and prediction of fluvial response to future climate change. After the rapid sea-level rise during the early Holocene, changes in discharge and/or sediment load due to climate changes might be dominant controls on floodplain evolution even in coastal areas, where the influence of sea-level is generally considered to be strong (McCabe and Shanley, 1992; Wright and Marriott, 1993; Blum and Törnqvist, 2000). Marriner et al. (2012a, b) indicated that the fluvial aggradation rates decreased in the Nile delta after 5000 cal BP, and inferred that it was related to low sediment production rate and low discharge due to the southward migration of Intertropical Convergence Zone. Giosan et al. (2012) inferred that weakening of Indian summer monsoon after ca. 5000 cal BP reduced sediment load compared to water discharge and this situation caused channel incision and stabilization, and formation of a large fluvial ridge in the Indus delta. Reconstructing a detailed floodplain chronology as well as comparison with allogenic controls with well constrained chronologies is required to clarify the response of the coastal floodplains to allogenic controls. Few studies reconstructed detailed floodplain chronologies because extensive field investigation is needed, and the susceptibility and response of coastal floodplains to allogenic controls in the middle to late Holocene is yet to be fully understood.

Fluvial sedimentation on coastal floodplains might be also susceptible to sea-level changes in the middle to late Holocene. Funabiki et al. (2012) argued that a decrease in accommodation due to stable sea-level during 6000–4000 cal BP and the subsequent sea-level fall led to slow aggradation in the Song Hong (Red River) delta, northern Vietnam. A similar fluvial response to sea-level changes is possible in other coastal floodplains because such changes in relative sea-level might have resulted

from the cessation of the eustatic sea-level rise around 4000 cal BP (Yokoyama et al., 2012, 2015). However, coastal floodplains in the East Asian summer monsoon (EASM) region, where Song Hong delta is located, could be also influenced by changes in discharge regime and sediment supply due to weakening of EASM in the middle to late Holocene. More research is needed to clarify the controls of the evolution of coastal floodplains during the middle and late Holocene.

The Ishikari lowland is a low-gradient fluvial and coastal lowland in western Hokkaido, northern Japan, in which peatlands are distributed between rivers (Figure 1). The Ishikari River floodplain is a favorable locality for investigating fluvial aggradation during the middle to late Holocene because the abundance of material in peat suitable for ^{14}C dating enables us to document the detailed chronology of the floodplain, and human impacts on the catchment is considered to be negligible before 1890s (e.g. Ahn et al., 2009). Ishii et al. (2014) demonstrated that the rapid sedimentation rates (7.6–12.1 mm/yr) before 7500 cal BP and subsequent decrease in sedimentation rates (0.7–2.5 mm/yr) at site IK1 (Figure 2) was probably related to the deceleration of sea-level rise. Although peat layers are found in various parts of the Holocene sequence in the Ishikari lowland, the widespread Uppermost Peat is the most prominent layer. This near-surface peat overlies clastic-dominated sediments. The Uppermost Peat has ^{14}C dates of ca. 4000–5000 calibrated years before present (cal BP) and is generally 3–5 m thick (Ishii et al., 2014; Matsushita et al., 1985; Miyaji et al., 2000). Sakaguchi (1974) first suggested that the onset of the Uppermost Peat represents a change from rapid to slower fluvial aggradation due to decreased avulsion frequency. Miyaji et al. (2000) argued that the onset of the Uppermost Peat around the city of Bibai (Figure 2) was associated with slower fluvial sedimentation beginning at 3500 yr BP. The onset of peat formation may reflect major fluvial response to allogenic controls in the middle to late Holocene.

The purpose of the study is to investigate the influence of sea-level and climate changes on fluvial aggradation in the middle to late Holocene based on analysis of 25 cores from the Ishikari lowland. We

introduce a new method to deal with the organic and clastic sedimentation rates separately, as well as plant macrofossil analysis, and demonstrate that the peat initiation reflects a change from rapid to slower fluvial aggradation rate and a lowering of water table. Furthermore, we reveal the floodplain evolution and compared the onset ages of the Uppermost Peat with sea-level and climate records to clarify the major allogenic control of the floodplain evolution. Our results contribute to an improved understanding of fluvial response to upstream allogenic controls in the middle to late Holocene, succeeding earlier sea-level control. All ages in this paper are reported as calibrated ^{14}C ages (cal BP) unless noted as yr BP.

Regional settings

Geomorphology

The Ishikari River (Figure 1) has a catchment area of approximately 14,330 km^2. Although the river is currently 268 km long, it was longer than 300 km before artificial cutoff projects for flood protection since 1910s.

The study area is located landward of the shoreline during the Holocene maximum transgression (Sagayama et al., 2010; Figure 1). The longitudinal gradient of its floodplain is gentle, approximately 0.00033–0.00020 (1/3000–1/5000) (Segawa et al., 2008). The area is characterized by a meandering channel, widespread peatlands, and oxbow lakes (Figure 2). Barriers developed near the Momijiyama Sand Dune (Figure 1) during the Holocene transgression (Sagayama et al., 2010), and at the time of the onset of the Uppermost Peat the lagoonal estuary was filled with sediment supplied mainly by the Ishikari River (Figures 1 and 2). The Holocene deposits are entirely fluvial in the study area. The uppermost part of the floodplain sediments generally consists of peat. The floodplain came under cultivation rapidly after the 1890s (Ahn et al., 2009), and the peatlands have been almost entirely removed today.

Present climate and hydrology

The summer precipitation in Japan is characterized by stationary fronts, called the Baiu and Akisame fronts, associated with the EASM. The Baiu front migrates northward slowly from May to August, and the Akisame front migrates southward from August to October. Hokkaido is located near the EASM front, and the maximum 5-day precipitation in Hokkaido occurs in late July because of the Baiu front (Matsumoto and Takahashi, 1999). The mean annual precipitation during the summer monsoon season (May–October) is approximately 550 mm. Although snowmelt floods occur in spring, large floods of the Ishikari River occur mainly in the summer monsoon season (Tada et al., 1961). Most of these large floods occur when typhoons approach the Baiu/Akisame fronts (Uehara and Takeda, 1982). Therefore, the EASM and typhoons influence precipitation in the drainage area, the discharge of the river, and the frequency and strength of floods in the Ishikari lowland.

The mean annual discharge at Tsukigata (1973–2013) is 340 m^3/s and the mean annual peak flow, occurring mainly during the summer monsoon season, is 3100 m^3/s. The annual maximum discharges and water levels (1975–2012) at Tsukigata, on the western side of the study area (Figure 2), are shown in Figure 3. The historical natural levee near Tsukigata, as shown on a topographic map from 1918, was approximately 12–14 m in elevation, and the river bed was 3–5 m in elevation in 1932 (Tada et al., 1961). Incision of the river bed by 1–2 m occurred between 1932 and 1950, but no incision has occurred since 1950. Therefore, overbank flooding may occur when the water surface rises above 12–14 m elevation and the discharge is approximately 3500–5000 m^3/s (Figure 3). Large floods that greatly exceeded the bankfull level occurred five times between 1975 and 2012 (Figure 3).

Sea-level history

The rate of eustatic sea-level rise averaged about 10 mm/yr between the last deglaciation and

7500–7000 cal BP, and it decelerated around 8000–7000 cal BP (Fleming et al., 1998; Peltier 2002; Milne and Peros, 2013). The eustatic sea-level rise was about 3–5 m between 7000 and 4000 cal BP (Fleming et al., 1998; Peltier 2002, 2004; Lambeck and Purcell, 2005; Bradley et al., 2011; Yokoyama et al., 2012, 2015; Milne and Peros, 2013; Lambeck et al,, 2014; Woodroffe et al., 2015).

Japan is a far-field location that experienced significant hydro-isostatic effects after the deceleration of sea-level rise around 7500–7000 cal BP. Indicators of past sea level around 6000–4000 cal BP are generally 1–3 m above present sea level because of crustal uplift due to hydro-isostatic effects in embayments in Japan (Nakada et al., 1991; Okuno et al., 2014). This means that the relative sea level stabilized around 6000–4000 cal BP and fell afterward, as suggested by geophysical numerical modeling (Nakada et al., 1991; Yokoyama et al., 1996, 2012, 2015; Okuno et al., 2014). Yokoyama et al. (2012, 2015) showed that the relative sea-level fall after around 4000 cal BP is likely related to the end of eustatic sea-level rise. Although the history of relative sea level in the Ishikari lowland has not been reconstructed, a radiocarbon age of 5350 ± 50 yr BP was obtained from *Corbicula japonica*, an indicator of past sea level, from Momijiyama Sand Dune (Figure 1) at 1.6 m elevation (Shiga, 2003). Diatom evidence also showed that the locality consists of marine deposits (Shiga, 2003). This evidence suggests that sea-level change in the Ishikari lowland was similar to that of other far-field areas, and not significantly affected by local tectonics.

Climate history

Many paleoclimate records from China indicated that the EASM was generally strong in the early to middle Holocene (An et al., 2000; Liu and Feng, 2012). A decrease in precipitation and temperature due to weakening of EASM from the middle to the late Holocene has been reported in many locations in the EASM region (An et al., 2000; Conroy et al., 2008; Dykoski et al., 2005; Hu et al., 2008; Xu et al., 2010; Liu and Feng, 2012). The most dramatic climate transition in the middle to late Holocene

occurred at around 4000 cal BP (Conroy et al., 2008; Liu and Feng, 2012).

Pollen analysis suggested that the temperature over Japan was generally higher than that of the present in the middle Holocene (Sakaguchi, 1981, 1993). A subsequent decrease in temperature occurred in 5000–3000 yr BP in the Ishikari lowland (Matsushita et al., 1985; Miyaji et al., 2000) and other areas in Japan (Sakaguchi, 1981, 1993). Such a temperature decrease in Japan may reflect weakening of the EASM.

Material and methods

At site IK1 (lat 43°19′52″N, long 141°46′13″E; elevation 14.2 m; penetration depth 26.3 m) (Ishii et al., 2014; Figure 2), a borehole core was obtained in September 2010 to evaluate the balance between organic and clastic sedimentation rates. The site is on the natural levee of the Old-bibai River. The sediment cores were split, photographed, described, and subsampled in the laboratory. Subsamples were collected at 10 cm intervals using polycarbonate containers (7 cm^3). We also obtained 24 cores up to 5 m long by using a hand-operated auger in August and September of 2012, 2013, and 2014 to investigate the ages and origins of the Uppermost Peat on the floodplain (cores numbered with the prefix "P" in Figure 2). Sediments were described in the field and subsampled at 5 cm intervals.

Wet and dry bulk densities of sediments were determined down core at site IK1. Wet bulk density was determined by weighing subsamples immediately after collection in polycarbonate containers, and dry bulk density was determined after drying the samples for 48 hours at 60 °C. Water content was calculated from these densities.

Total organic content was estimated from loss on ignition (LOI). Approximately 0.5–3 g sediment was weighed and dried at 80 °C for 48 hours, then heated in an electric muffle furnace at 750 °C for 1 hour. LOI is often used for classification of soil types, including peat (e.g., Wüst et al., 2003). In this study, samples with a LOI greater than 20% were classified as peat (van Asselen et al.,

2010), and we classified sediments with LOI values of 10–20% and less than 10% as organic-rich mud and mud, respectively.

Plant macrofossils (fruits and seeds) were analyzed to identify sedimentary environment changes before and after the formation of the Uppermost Peat had commenced. We gently washed 5–12.5 cm^3 samples of sediments on a sieve with 0.35 mm mesh. Fruits and seeds were picked from the residue on the sieve, then identified and counted under a binocular microscope.

^{14}C analysis was conducted on plant fragments and wood pieces using accelerator mass spectrometry (Table 1). The samples were cleaned in an ultrasonic bath with distilled water and then processed by the standard acid-alkali-acid (AAA) treatment. The samples were combusted in sealed Vycol tubes with copper oxide at 850 °C. The evolved CO_2 was separated cryogenically and reduced to graphite on an iron catalyst with hydrogen gas (Kitagawa et al., 1993). The graphite samples from core IK1 were measured at KIGAM (Korean Institute of Geoscience and Mineral Resources), and the other graphite samples were submitted to the Keck-Carbon Cycle AMS Facility (University of California, Irvine) and DirectAMS laboratory. Four samples were submitted to Paleo Labo Co., Ltd. before the AAA pretreatment. The ages were calibrated using OxCal 4.2 (Bronk Ramsey, 2009) based on atmospheric data from Reimer et al. (2013). We obtained 18 radiocarbon dates (including the age obtained from core IK1) from near the base of the Uppermost Peat to clarify the onset ages of the peat (Table 2). The sum of the probability densities of these radiocarbon ages were obtained using OxCal 4.2.

Sedimentation rates (mm/yr) in core IK1 were estimated based on the median probability of the two sigma range for each sample. An age-depth model was constructed based on the median probability of the calibrated ^{14}C ages. The effect of any type of compaction was ignored in the age-depth model.

Clastic sedimentation rates in core IK1

The initiation of peat deposition on a floodplain may be controlled by altered rates of clastic sedimentation, changing the mixing ratio of in situ produced organic materials (Bohacs and Suter, 1997). Therefore, we determined the rates of clastic sedimentation before and after the peat initiation, and evaluated the influence of reduced clastic sedimentation rates on the initiation of peat formation. The clastic sedimentation rate of core IK1 ($SR_{clastic,\ IK1}$, cm/yr) was determined using the following equations (equations 1 and 2):

$$SR_{clastic,\ IK1} = F_{clastic,\ IK1} / \rho_{clastic} \quad (1)$$

$$F_{clastic,\ IK1} = \rho_{IK1} \times (1 - LOI_{IK1}) \times SR_{IK1} \quad (2)$$

where $F_{clastic,\ IK1}$ is the clastic sediment flux in core IK1 (g/cm^2/yr), $\rho_{clastic}$ is the dry bulk density of uncompacted clastic sediment (g/cm^3), ρ_{IK1} is the dry bulk density of the collected samples, and SR_{IK1} is the sedimentation rate estimated from depths and calibrated ^{14}C ages. The errors of $F_{clastic,\ IK1}$ reflect the maximum and minimum values of SR_{IK1} calculated from the 2 sigma errors of calibrated ^{14}C ages. The grain sizes of the overbank deposits at 6.4–7.0 m depth in core IK1 are very fine silt and clay (around 8 φ), similar to the grain size of clastic sediments included in peat. Based on the average dry bulk density of these sediments, which is representative for mildly compacted overbank sediments in core IK1, we used 0.8 g/cm^3 as the value for $\rho_{clastic}$. When we calculate the $SR_{clastic,\ IK1}$, the effect of compaction included in SR_{IK1} is corrected, by multiplying SR_{IK1} by ρ_{IK1} in equation (2).

LOI and the balance between organic and clastic sedimentation rates

We assessed the relationship between clastic sedimentation rate and LOI obtained from the analysis of

core IK1 by comparison with theoretical values. LOI, which mainly reflects the proportion of organic sediments (plant residues), is can be approximated by the balance between organic and clastic sedimentation (equation 3; e.g. Lorenzo-Trueba et al., 2012):

$$LOI = P_{organic} / (F_{clastic} + P_{organic}) \quad (3)$$

where $P_{organic}$ is organic production rate (g/cm^2/yr) and $F_{clastic}$ is clastic flux (g/cm^2/yr). Furthermore, we estimated the clastic sedimentation rate ($SR_{clastic}$, cm/yr) and organic sedimentation rate ($SR_{organic}$, cm/yr) using the following equations (equations 4 and 5):

$$SR_{clastic} = F_{clastic} / \rho_{clastic} \quad (4)$$

$$SR_{organic} = P_{organic} / \rho_{peat} \quad (5)$$

where ρ_{peat} is the dry bulk density of pure uncompacted peat (LOI ≅ 100). We determined ρ_{peat} as 0.09354 g/cm^3 using the following empirical formula (equation 6; van Asselen et al., 2010):

$$\rho_{peat} = 0.6641 \exp(-0.0196\ LOI) \quad (6)$$

The equation could be used to calculate the dry bulk density of fen peat composed of herbaceous and woody material in cold temperate settings (van Asselen et al., 2010). The fractional uncertainty of the formulation is estimated to be 10% (van Asselen et al., 2010).

Results

Characteristics and interpretation of the sediments

The sedimentary facies of our auger samples and core IK1 show that the uppermost part of the floodplain sediments is mainly composed of peat generally 3–5 m thick underlain by fluvial clastic sediments (Figures 4 and 5), consistent with the findings of previous studies (Matsushita et al., 1985; Miyaji et al., 2000; Sakaguchi, 1974). In this study, we generally placed the base of the Uppermost Peat at the base of the near-surface thickest peat unit which does not include clastic-dominated sediments more than 20 cm thick except at sites P23, P42, and IK1, where the Uppermost Peat includes organic-rich mud several tens of centimeters thick (Figures 4 and 5). Below the Uppermost Peat, beds of organic-rich mud or clay thicker than 20 cm is underlain by peat at sites P1, P11, P24, P47, and IK1 (Figures 4 and 5). Thin alternating beds of mud and peat were present near the base of the Uppermost Peat at sites P2 and P46 (Figure 4). Silt-clay layers as thick as several centimeters were intercalated in the uppermost 1 m of the peat at sites P1, P13, P16, P19, P45, and P46 (Figure 4), although almost these locations are not so close to rivers (Figure 2). At site IK1, on the natural levee, layers of organic-rich mud or very fine sand intercalated in peat were younger than 1700 cal BP (Figure 5).

The LOI of peat is between 20% and 99% (Figure 4). To the naked eye, peat appeared fibrous in sediment with high LOI and overbank clastic components were relatively abundant in sediment with low LOI. Peat consisted mostly of basal sheaths, rhizomes, and roots of herbaceous plants with occasional wood fragments. The uppermost part of the peat where the LOI was >90% at site P16 was mainly composed of sphagnum moss.

Massive bluish gray clay without pedogenic features (LOI < 10%) or gray organic-rich mud (LOI = 10–20%) underlies the Uppermost Peat at all sites except P13 and P6 (Figure 4). Organic-rich mud contained relatively abundant plant fragments. A few rootlets and plant fragments were found in the bluish gray clay layer at sites P23, P24, P42, P46, and IK1, but were generally rare at the other sites

(Figures 4 and 5). Wood fragments were found in the clay at sites P16, P23, P24, P46, and IK1 (Figures 4 and 5). In core IK1, large wood fragments were restricted to 9.2–8.3 m depth (Figure 5). Vivianite nodules were locally present in the clay at sites P23 and P44 (Figure 4). We interpreted the clay and organic-rich mud as overbank deposits, because fine-grained deposits with plant fragments and rootlets are typical of floodbasin deposits (Aslan and Autin, 1999) and diatom assemblages indicated that the area is landward of the shoreline during the Holocene transgression (Sagayama et al., 2010). The presence of vivianite in the clay at sites P23 and P44 suggests that the floodbasin was poorly drained (Aslan and Autin, 1999).

The deepest part of sites P6, P12, P13, P19, and P41 consisted of sandy silt to silty sand (Figure 4). The LOI of this sediment was generally less than 5% (Figure 4). At site P6, alternating beds of sandy silt and silty sand several decimeters thick were found that rapidly fined upward at the top of the layer (Figure 4). Wood fragments and plant fragments were very rare in this material except at site P41 (Figure 4). The sparse distribution of the sandy deposits implies that these deposits are associated with small-scale crevasse splays or natural levees.

Artificial soil is spread on agricultural land and natural soils are present in forested land (Figure 4). The LOI of artificial and natural soils is generally less than 50% (Figure 4). The artificial and natural soils generally include decomposed peat.

Geochronology and sedimentation rates

We obtained 18 ^{14}C dates from samples within 0.3 m of the base of the Uppermost Peat (Table 2). We calculated the sedimentation rates using the median probability of calibrated ^{14}C ages (Table 2). Moreover, we estimated the onset ages of the Uppermost Peat by interpolation or extrapolation of the sedimentation rates (Table 2). Most of the Uppermost Peat began to form between 5600 and 3600 cal BP, and the ages appear to be concentrated at 5600–5000, 4600–4300, and 4100–3600 cal BP (Table 2).

The Uppermost Peat began to form around 5600–5000 cal BP at sites P13, P15, P16, P18, P42, and IK1; around 4600–4300 cal BP at sites P25 and P46; and around 4100–3600 cal BP at sites P1, P2, P3, P6, P11, P12, P19, P23, P24, and P45 (Figures 2 and 4; Table 2). The different onset ages were found in the west of the Old-bibai River, whereas 4100–3600 cal BP onset ages for the Uppermost Peat are clustered in the east of the river (Figure 2). The basal dates of the Uppermost Peat were not obtained at sites P14, P21, P22, P40, P41, P44, and P47 (Figure 4). The onset ages are considered to be older than 4100–3600 cal BP at sites P14 and P21 (Figure 4).

Before 4100–3600 cal BP, alternations of peat and organic-rich mud occurred at some locations. Peat occurs below the Uppermost Peat at sites P1, P11, and P24, where the Uppermost Peat began to form around 4600–4300 or 4100–3600 cal BP (Figure 4). The onset ages of the lower peat were not obtained at these sites. At site IK1, a peat layer with onset ages around 6500 cal BP are present below the Uppermost Peat. At sites P42 and IK1, the organic-rich mud occurred in the Uppermost Peat before 4100–3600 cal BP, while organic-rich mud layers were formed after 4100–3600 cal BP at site P23. The intercalation of organic-rich mud layers in the Uppermost Peat at site P23 may have resulted from the close proximity to a tributary river.

The sedimentation rate at site IK1 was 1.5 mm/yr during 6900–6300 cal BP and increased to 5.1 mm/yr during 6300–5900 cal BP (Figure 5a). This increase in sedimentation rate was accompanied by upward coarsening of the overbank sediments (Figure 5). The sedimentation rate gradually decreased after ~5900 cal BP and reached a minimum of 0.7–1.0 mm/yr between 5200 and 1700 cal BP (Figure 5a). This was the period when peat formation predominated (Figure 5b). After 1700 cal BP, the deposition of the natural levee was accompanied by an increase in sedimentation rate to 2.0–2.2 mm/yr (Figure 5).

Plant macrofossil analysis

The results of the plant macrofossil analysis are shown in Figure 6. All of the plant species represented grow in wetlands, except for *Achillea* sp. and *Ampelopsis brevipedunculata*, remains of which may have been transported from mesic habitats. Among the wetland plants, *Potamogeton* sp. is a submergent plant indicating a shallow lake environment, and *Schoenoplectus* sp. and *Menyanthes trifoliata* are emergent plants growing in very shallow water. Sedges (*Carex* spp.) are typical peat-forming plants that grow densely at the present research site; we classified the macrofossils into *Carex* sect. *Stellulatae*, *Carex* sect. *Phacocystis*, and *Carex* spp. type A based on fruit morphology. *Carex* spp. type A are fruits with a typical triangular transverse section. The plant species identified in this study is generally found in Eurasian peatlands (Sakaguchi, 1974).

At site P43, the occurrence of *Potamogeton* sp. in the clay layer at 445–450 and 475–480 cm depth, plus the dominance of *Schoenoplectus* sp. at 435–450 cm and *Carex* spp. and *Triadenum japonicum* at 425–435 cm, together indicate a gradual decrease in water depth around the site (Figure 6g). At site P45, the occurrence of *Menyanthes trifoliata* near the base of the Uppermost Peat suggests that the water table was above the surface before the onset of deposition of the Uppermost Peat (Figure 6d).

Carex spp. occurred at or just below the base of the peat at sites P13 and P19 (Figure 6a, b), indicating that *Carex* communities were established at or near the site of peat deposition. On the other hand, *Carex* fruits in the underlying clay and organic-rich mud were accompanied by relatively abundant autochthonous plant fragments at site P25 (435–440 and 455–460 cm depth; Figure 6c), site P46 (435–440 and 475–480 cm depth; Figure 6e), and site IK1 (650–655, 675–680, and 695–700 cm depth; Figure 6f). Because these sediments also included plants growing on sunny shorelines in tall sedge assemblages, such as *Menyanthes trifoliata* (395–400 cm depth at site P25; Figure 6c), *Eriocaulon* sp. (455–460 cm depth at site P46; Figure 6e), and *Schoenoplectus* sp. (1035–1040 cm depth at site IK1; Figure 6f), the sediments may represent a very shallow subaquatic environment and

the *Carex* fruits were possibly transported from the shore. These results show that the typical peat-forming plant like *Carex* communities hardly existed before peat deposition.

Discussion

LOI and the balance between clastic and organic sedimentation rates

Figure 7 plots the clastic sedimentation rate $SR_{clastic}$ against LOI in core IK1 along with three curves showing the calculated relationship between clastic sedimentation rate and LOI, based on equations (3)–(5), for organic sedimentation rates of 0.5, 1.0, and 1.5 mm/yr. The underlying calculation of clastic sedimentation flux $F_{clastic, IK1}$ in equation (2) relies on a sedimentation rate SR_{IK1} based on ^{14}C ages, which might result in significant errors because the calibrated ages have uncertainties of several hundred years (Table 1). For example, the relatively large errors of clastic sedimentation rates between 6.3–7.4 m (Figure 7) resulted from large SR_{IK1} (Figure 5). In contrast, the errors of clastic sedimentation rates between 3.6 and 6.3 m depth, representing peat and organic-rich mud (open symbols in Figure 7), are relatively small because SR_{IK1} is inherently small during peat deposition (Figure 7).

Accurate estimation of the net accumulation rate of wetland plants is highly complicated because it is associated with the primary production rate as well as the decay rate (Charman, 2002). However, accumulation rates of peat are generally associated with climate zone when calculated over multiple centuries to millennia, including autocompaction over that time window, being about 1–2 mm/yr in warm-temperate zones and less than 1 mm/yr in cool-temperate zones (Bohacs and Suter, 1997). Hence, it is reasonable to assume that the organic sedimentation rate in equation (5) is less than 1 mm/yr in the cool-temperate Ishikari lowland.

The $SR_{clastic}$ values obtained from 3.6–6.3 m depth in core IK1 are fairly consistent with the theoretical values calculated from equations (3)–(5), whereas those obtained from depths above and

below this level generally are higher than the theoretical values (Figure 7). Above 3.6 m and below 6.3 m depth, core IK1 includes overbank deposits as well as peat, and relatively higher sedimentation rates associated with the overbank deposits might lead to overestimation of $SR_{clastic}$ values in the peat (equation 2). Moreover, $SR_{clastic}$ values in the 0.4–3.6 and 7.5–10.3 m depth ranges may be overestimated because the value for dry bulk density of clastic sediments, $\rho_{clastic}$, used in equation (1) (0.8 g/cm^3) is lower than the actual values because the overbank deposits at these depths are coarser grained than 8φ (Figure 5).

Despite the uncertainties just noted, Figure 7 shows that as the clastic sedimentation rate decreases, LOI generally increases. The clastic sedimentation rate decreased from 0.9–2.0 mm/yr at 6.3–7.4 m to less than 0.6 mm/yr at 5.7–6.3 m depth, and peat formation became dominant at 5.7–6.3 m depth. This indicates that the clastic sedimentation rate is less than 0.6 mm/yr when peat (LOI > 20%) is formed.

The initiation of the Uppermost Peat around 4300 cal BP roughly coincides with the decrease in clastic sedimentation rate at site IK1 (Figure 5 and 7), and the decrease in clastic components at the base of the Uppermost Peat is also reflected in the increase in LOI of auger cores (Figure 4). Likewise, the clastic sedimentation rate was relatively low during earlier peat deposition around 6500 cal BP at site IK1, although the clastic sedimentation rate during the peat deposition might be overestimated. The reason for that is the presence of overbank deposits as well as peat between 9.3 and 10.3 m depth (Figure 7), which might lead to higher SR_{IK1} in equation (2). The steep gradient of the curve in Figure 7 between 10% and 20% LOI, when peat formation begins, signifies that the fluvial aggradation rate must have decreased substantially during the deposition of the widespread Uppermost Peat.

Changes in water table

In general, peat initiation on floodplains is controlled by the water table in the summer growing season as well as the clastic sedimentation rate (Bohacs and Suter, 1997). Peat does not form when the water is

too deep or the water table is too low because peat-forming plants like sedge are not generally tolerant of high water level or drought. For example, peat deposition in Cumberland Marshes, Canada, in the last 3000 years is believed to have followed up the shallowing and infilling of floodplain lakes by avulsive deposits and subsequent abandonment and isolation from active channels (Morozova and Smith, 1999).

The absence of *Carex* spp. below the Uppermost Peat at sites P13, P19, P43, and P45 (Figure 6a, b, d, g) suggests that the sedimentary environment around these locations was not suitable for the establishment of *Carex* communities. At site P43 (Figure 6g), the changes from the presence of *Potamogeton* sp. (445–450 and 475–480 cm) to the dominance of *Schoenoplectus* sp. (435–450 cm), followed by the dominance of *Carex* spp. (430–435 cm) with *Triadenum japonicum* (425–435 cm), indicate that a gradual decrease in the water depth promoted the growth of *Carex* spp. Furthermore, although *Carex* occurred in the underlying clay and organic-rich mud at some sites, the presence of *Menyanthes trifoliata* (395–400 cm at site P25; Figure 6c), *Eriocaulon* sp. (455–460 cm at site P46; Figure 6e), and *Schoenoplectus* sp. (1035–1040 cm at site IK1; Figure 6f) suggests a shallow lake environment, at least in the summer growing season, before the onset of the Uppermost Peat. These changes imply that peat formation was associated with decrease in the water depth of floodplain lakes in the growing season.

If the onset of the Uppermost Peat was due to the infilling and shallowing of floodplain lakes, the altitudes of the onset of the Uppermost Peat would be almost the same level. However, the altitudes of the onset of the Uppermost Peat increase with time (Figure 8a). This indicates that the water level of the floodplain remained high without infilling and shallowing of floodplain lakes whereas the vertical accretion of fluvial sediments continued at each location before the onset of the Uppermost Peat. Therefore, the decrease in water depth of the floodplain lakes before the peat initiation resulted from the lowering of lake level.

While the decreased fluvial aggradation is considered to have led to the peat initiation, the lowering of water level also appears to be important to the onset of the peat formation. Therefore, we infer that both a lowering of water level in the growing season and a decrease in overbank sedimentation rate at each location led to initiation of the Uppermost Peat in the Ishikari lowland.

Floodplain evolution

The dates of initiation of the Uppermost Peat are not synchronous but are concentrated at 5600–5000, 4600–4300, and 4100–3600 cal BP (Table 2). The peat initiation due to the lowering of water level and decrease in overbank sedimentation rate at each location may be associated with autogenic and/or allogenic controls. The floodplain evolution needs to be discussed before it is linked to possible allogenic controls.

While crevasse splays or natural levees are sparsely present below the Uppermost Peat, they are almost absent above the base of the Uppermost Peat at each location (Figures 2 and 4). This may indicate that the Uppermost Peat initiation is associated with the abandonment of crevasse splays or natural levees. Because crevasse splays contain multiple distributary channels that route water and sediment to and beyond the splay margins (Bristow et al., 1999; Slingerland and Smith, 2004; Lewin and Ashworth, 2014), the presence of crevasse splays increases the flood frequency and promotes overbank sedimentation in the further floodbasin. Furthermore, the water supply from rivers to the floodplain accounts for large portions of the lake water (e.g. Lesack and Melack, 1995; Bonnet et al., 2008; Brock et al., 2009), and frequent overbank floods might have resulted in high water level in the floodplain lakes in the summer growing season. Therefore, the abandonment of crevasse splays might lead to the Uppermost Peat initiation in the Ishikari lowland. The abandonment of crevasse splays may have resulted in decreased avulsion frequency, as inferred by Sakaguchi (1974).

The onset of the Uppermost Peat was not synchronous in the west of the Old-Bibai River while

the peat initiation is relatively synchronous in the east of the Old-bibai River (Figure 2). Moreover, peat was found below the Uppermost Peat at sites P1, P11, P24, and IK1, and the Uppermost Peat includes organic-rich mud before 4100–3600 cal BP at sites P42 and IK1 (Figures 4 and 5). The asynchronous onset of the Uppermost Peat and the interbedded peat and organic-rich mud or clay before 4100–3600 cal BP might reflect the spatial distribution of the crevasse splays and differences in the timing of the abandonment of the crevasse splays.

Although the crevasse splay or natural levee deposits were only found at P12 (Figures 2 and 4), we infer that small crevasse splays were also present in the east of the Old-bibai River before the onset of the Uppermost Peat because of the presence of many tributaries from the mountain. The relatively delayed onset of the Uppermost Peat around 4100–3600 cal BP in the area (Figure 2) suggests delayed abandonment of crevasse splays of the tributaries. At the same time, it means that the onset of the Uppermost Peat around 4100–3600 cal BP at sites P1, P19, and P24 in the west of the Old-bibai River (Figure 2) might be associated with the abandonment of crevasse splays of tributaries.

The sum of the probability densities of the basal dates for the Uppermost Peat shows peaks around 5600–5000, 4600–4300, and 4100–3600 cal BP (Figure 8b). In particular, the sum of the probability densities of the calibrated ages obtained from samples within 0.1 m of the base of the peat shows clearer peaks (Figure 8b). These suggest that an allogenic control promoted the abrupt abandonment of most of the crevasse splays in the study area. Furthermore, the delayed abandonment of the crevasse splays of the tributaries around 4100–3600 cal BP may be explained by different responses of the Ishikari River and its tributaries to the allogenic control.

Cause of decreased fluvial aggradation

The formation and abandonment of crevasse splays in coastal floodplains may be influenced by allogenic controls such as sea-level and climate changes. Stable relative sea-level and the subsequent

fall in sea-level might have decreased the accommodation and led to abandonment of natural levees and crevasse splays (e.g. Funabiki et al., 2012), although Nijhuis et al. (2015) demonstrated that fluvial systems could remain aggradational during relative sea-level fall based on results of a numerical simulation and a field research in Goose River, Canada. On the other hand, a weakening of the EASM in the middle to late Holocene (An et al., 2000; Dykoski et al., 2005; Conroy et al., 2008; Hu et al., 2008; Xu et al., 2010; Liu and Feng, 2012) might have resulted in the abandonment of the crevasse splays because deposition of crevasse splay deposits may be associated with changes in flood discharge due to changes in precipitation (Aalto et al., 2003), while allogenic controls are not necessarily most significant factors for the deposition of crevasse splay deposits (Shen et al., 2015). A detailed comparison of allogenic controls and the floodplain evolution is needed because sea-level and climate changes could have similar influence on the fluvial aggradation.

The delayed abandonment of the crevasse splays of the tributaries around 4100–3600 cal BP may be attributed to different responses of the Ishikari River and its tributaries to an allogenic control. Influence of sea-level changes might be delayed in the tributaries because a propagation of the downstream control to the upstream seems more difficult for the steep-gradient tributaries than the low-gradient Ishikari River. Therefore, sea-level changes might explain the delayed onset ages around 4100–3600 cal BP. On the other hand, runoff responses of the different-sized catchments may also explain the differences in the timing of the abandonment of the crevasse splays. The tributaries sometimes flood even when the Ishikari River does not flood (Tada et al., 1961) because intense precipitation only in local areas leads to the floods of the tributaries with small-sized catchments (generally <200 km^2). Similar delayed responses of the tributaries to sea-level and climate changes are possible, and we can't specify the significant allogenic control of the floodplain evolution based on the mechanisms responsible for the differences in the timings of the abandonment of the crevasse splays. To do so in the future discussion, we would need a more detailed comparison of the timings of the

changes in allogenic controls and the floodplain evolution.

Previous studies demonstrated that eustatic sea-level decelerated around 5000–4000 cal BP (e.g. Bradley et al., 2011), which is relatively close to the onset ages of the Uppermost Peat (Figure 8b, d). However, Lambeck et al. (2014) showed that there is no evidence for oscillations in eustatic sea-level exceeding 15–20 cm over time intervals of ≥200 years between 6000 and 150 cal BP. Such small changes in eustatic sea-level appears to be insignificant to the formation and abandonment of crevasse splays in the Ishikari lowland.

The relative sea-level change at a given location after 7000 cal BP strongly reflects glacio-hydro-isostatic effects, isostatic movements triggered by sediment loading, tectonic activity, and sediment compaction. Although relative sea-level fall after 6000–4000 cal BP is considered to result from the cessation of eustatic sea-level rise (Yokoyama et al., 2012, 2015) and generally recognized as a smooth multimillennial trend (Sato, 2008; Tanabe et al., 2003; Yokoyama et al., 1996), some coastal studies in Japan have shown that a relative sea-level fall of a few meters could have occurred over a span of several centuries to a millennium between 5000 and 2000 cal BP (Kawase, 1998; Ohira and Umitsu, 1999; Ono, 2004; Ota et al., 1990 and references therein; Tanabe et al., 2013). In the innermost areas of the Tonegawa Lowland, Tanabe et al. (2016) noted that a relative sea-level fall due to isostatic movements triggered by sediment loading might have occurred during 4000–3000 cal BP, a time interval that is close to the initiation of the Uppermost Peat at 4100–3600 cal BP. However, at present, no submillennial sea-level fluctuations that correspond to the three initiation dates of the Uppermost Peat have been reported in coastal lowlands of Japan. We infer that another controlling factor is associated with the change from rapid to slower fluvial aggradation around 5600–5000, 4600–4300, and 4100–3600 cal BP in the Ishikari lowland.

Overbank floods occur in the Ishikari lowland mainly in response to precipitation by the Baiu/Akisame fronts and typhoons in the summer monsoon season (Tada et al., 1961), and changes in

EASM strength may be associated with the formation and abandonment of crevasse splays. The decrease in precipitation in the EASM region appears as a submillennial fluctuation in high-resolution speleothem records in China (e.g. Dykoski et al., 2005; Hu et al., 2008). The low $\delta^{18}O$ values of stalagmite records are generally consistent with strong summer monsoon because $\delta^{18}O$ of rainwater is inversely correlated to amount of rainfall (Hu et al., 2008). Positive shifts in $\delta^{18}O$ at around 5600 and 3800 cal BP suggest that two major decreases in precipitation occurred in the middle and late Holocene (Dykoski et al., 2005; Figure 8c). The basal Uppermost Peat dates of 5600–5000, 4600–4300, and 4100–3600 cal BP largely correspond to the weakening of the EASM (Figure 8b, c). The last prominent weakening event in the mid to late Holocene transition agrees with the most widely represented initiation date for the Uppermost Peat around 4100–3600 cal BP in the Ishikari lowland (Figure 8b, c). Furthermore, the deposition of the Uppermost Peat was not interrupted by overbank sediments after this weakening except at site P23 (Figure 4). We consider that the slower fluvial aggradation due to the abandonment of crevasse splays around 5600–5000, 4600–4300, and 4100–3600 cal BP in the Ishikari lowland were strongly related to decreases in precipitation from a weakened EASM. This in turn suggests that fluvial aggradation on floodplains is susceptible to submillennial-scale fluctuations in climate.

It is possible that the fluvial aggradation rate of other coastal lowlands decreased due to weakening of the EASM around 5600–3600 cal BP. For example, Ohira (1995) argued that a fall in the groundwater table due to rapid relative sea-level fall may be an important factor for peat initiation around 4500–4000 yr BP in the Sarobetsu coastal lowland, Hokkaido, northern Japan. Ohira (1995) did not consider the influence of fluvial aggradation on the peat initiation. However, decreased precipitation from a weakened EASM and subsequent decreasing fluvial aggradation and lowering water level of the floodplain, also may have contributed to peat initiation. Moreover, in the inner part of the Song Hong (Red River) delta of northern Vietnam, the decrease in fluvial aggradation rate during

6000–4000 cal BP may have been influenced by weakening of the EASM, although Funabiki et al. (2012) suggested that the decrease was due to limited accommodation associated with a stable sea level at that time. However, the changes in the fluvial aggradation rate in multi-centennial scale are not confirmed in these studies. More well-constrained chronologies of coastal floodplains in the EASM region can help clarify the influence of regional climate changes on floodplain evolution.

Conclusions

We analyzed the decreased fluvial aggradation in the middle to late Holocene based on data from 25 cores that included LOI measurements, ^{14}C dates, estimates of clastic sedimentation rates, and plant macrofossil analyses. The middle to late Holocene initiation of the Uppermost Peat is probably associated with a decrease in fluvial aggradation rate and lowering of the water table. This initiation event occurred during three periods: 5600–5000, 4600–4300, and 4100–3600 cal BP. Onset ages for the three events were found in the west of the Old-bibai River, whereas 4100–3600 cal BP onset ages are clustered in the east of the river. From our comparison of this chronology with the EASM records, we infer that regional climate changes occurring at submillennial time scales significantly contributed to the decreased fluvial aggradation. Furthermore, the spatial differences in the timing of Uppermost Peat initiation events may result from the distribution of the crevasse sprays and runoff responses of different-sized catchments in the Ishikari lowland. Our results imply that fluvial aggradation of other floodplains in the EASM region also may have been significantly influenced by the weakening of EASM around 5600–3600 cal BP.

Acknowledgements

We thank Hiroyuki Kitagawa of Nagoya University for preparing graphite samples for ^{14}C analysis. We thank the landowners in the Ishikari lowland for allowing us access to their land. We greatly

appreciate the assistance of Nobuaki Ito and Eito Takahashi in the field. This paper greatly benefited from the extensive comments and suggestions of Kim Cohen and an anonymous reviewer.

Funding

This work was supported by the 10th Paleo Labo Young Researcher Science Grant, a Grant-in-Aid for JSPS Fellows (15J01971), and Scientific Research Project (No. 22680059) of the Ministry of Education, Culture, Sports, Science and Technology of Japan.

References

Aalto R, Maurice-Bourgoin L, Dunne T et al. (2003) Episodic sediment accumulation of Amazonian flood plains influenced by El Niño/Southern Oscillation. *Nature* 425: 493–497.

Ahn YS, Nakamura F, Kizuka T et al. (2009) Elevated sedimentation in lake records linked to agricultural activities in the Ishikari River floodplain, northern Japan. *Earth Surface Processes and Landforms* 34: 1650–1660.

An Z, Poter SC, Kutzbach JE et al. (2000) Asynchronous Holocene optimum of the East Asian monsoon. *Quaternary Science Reviews* 19: 743–762.

Aslan A and Autin WJ (1999) Evolution of the Holocene Mississippi River floodplain, Ferriday, Louisiana: Insights on the origin of fine-grained floodplains. *Journal of Sedimentary Research* 69: 800–815.

Blum MD and Törnqvist TE (2000) Fluvial responses to climate and sea-level change: a review and look forward. *Sedimentology* 47: 2–48.

Bohacs K and Suter J (1997) Sequence stratigraphic distribution of coaly rocks: fundamental controls and paralic examples. *AAPG Bulletin* 81: 1612–1639.

Bonnet MP, Barroux G, Martinez JM et al. (2008) Flooplain hydrology in an Amazon floodplain lake

(Lago Grande de Curuaí). *Journal of Hydrology* 349: 18–30.

Bradley SL, Milne GA, Shennan I et al. (2011) An improved Glacial Isostatic Adjustment model for the British Isles. *Journal of Quaternary Science* 26: 541–552.

Bristow CS, Skelly, RL and Ethridge FG (1999) Crevasse splays from the rapidly aggrading, sand-bed, braided Niobrara River, Nebraska: effect of base-level rise. *Sedimentology* 46: 1029–1047.

Brock BE, Yi Y, Clogg-Wright KP et al. (2009) Multi-year landscape-scale assesment of lakewater balances in the Slave River Delta, NWT, using water isotope tracers. *Journal of Hydrology* 379: 81–91.

Bronk Ramsey C (2009) Bayesian analysis of radiocarbon dates. *Radiocarbon* 51: 337–360.

Charman D (2002) *Peatlands and Environmental Change*. Chichester: John Wiley & Sons Ltd.

Conroy JL, Overpeck JT, Cole JE et al. (2008) Holocene changes in eastern tropical Pacific climate inferred from a Galápagos lake sediment record. *Quaternary Science Reviews* 27: 1166–1180.

Dykoski CA, Edwards RL, Cheng H et al. (2005) A high-resolution, absolute-dated Holocene and deglacial Asian monsoon record from Dongge Cave, China. *Earth and Planetary Science Letters* 233: 71–86.

Fleming K, Johnston P, Zwartz D et al. (1998) Refining the eustatic sea-level curve since the Last Glacial Maximum using far- and intermediate-field sites. *Earth and Planetary Science Letters* 163: 327–342.

Funabiki A, Saito Y, Phai VV et al. (2012) Natural levees and human settlement in the Song Hong (Red River) delta, northern Vietnam. *The Holocene* 22: 637–648.

Giosan L, Clift PD, Macklin MG et al. (2012) Fluvial landscapes of the Harappan civilization. *Proceedings of National Academy of Sciences USA* 109: E1688–E1694.

Hu C, Henderson GM, Huang J et al. (2008) Quantification of Holocene Asian monsoon rainfall from spatially separated cave records. *Earth and Planetary Science Letters* 266: 221–232.

Ishii Y, Ito A, Nakanishi T et al. (2014) Changes in sedimentary environment and sedimentation rate of the IK1 core obtained from the inner part of Ishikari lowland, northern Japan. *The Quaternary Research (Daiyonki Kenkyuu)* 53: 143–156 (in Japanese with English abstract).

Kawase K (1998) Late Holocene Paleoenvironmental changes in the Yahagi River lowlands, central Japan. *Geographical Review of Japan* 71: 411–435 (in Japanese with English abstract).

Kitagawa H, Masuzawa T, Nakamura T et al. (1993) A batch preparation method for graphite targets with low background for AMS 14C measurements. *Radiocarbon* 35: 295–300.

Lambeck K and Purcell A (2005) Sea-level change in the Mediterranean Sea since the LGM: model predictions for tectonically stable areas. *Quaternary Science Reviews* 24: 1969–1998.

Lambeck K, Rouby H, Purcell A et al. (2014) Sea level and global ice volumes from the Last Glacial Maximum to the Holocene. *Proceedings of National Academy of Sciences USA* 111: 15296–15303.

Leseck LF and Melack JM (1995) Flooding hydrology and mixture dynamics of lake water derived from multiple sources in an Amazon floodplain lake. *Water Resources Research* 31: 329–345.

Lewin J and Ashworth PJ (2014) The negative relief of large river floodplains. *Earth Science Review* 129: 1–23.

Liu F and Feng Z (2012) A dramatic climatic transition at ~4000 cal. yr BP and its cultural responses in Chinese cultural domains. *The Holocene* 22: 1181–1197.

Lorenzo-Trueba J, Voller VR, Paola C et al. (2012) Exploring the role of organic matter accumulation on delta evolution. *Journal of Geophysical Research* 117: F00A02

Marriner N, Flaux C, Kaniewski D et al. (2012a) ITCZ and ENSO-like pacing of Nile delta hydro-geomorphology during the Holocene. *Quaternary Science Reviews* 45: 73–84.

Marriner N., Flaux C., Morhange C et al. (2012b) Nile Delta's sinking past: Quantifiable links with Holocene compaction and climate-driven changes in sediment supply? *Geology* 40: 1083–1086.

Matsumoto J and Takahashi K (1999) Regional differences of daily rainfall characteristics in East

Asian summer monsoon season. *Geographical Review of Japan* 72B: 193–201.

Matsushita K, Igarashi Y and Umeda Y (1985) Genesis and transfiguration of the Ishikari peat-land in Hokkaido. *Report of the geological survey of Hokkaido* 70: 71-88 (in Japanese with English abstract).

McCabe PJ and Shanley KW (1992) Organic control on shoreface stacking patterns: Bogged down in the mire. *Geology* 20: 741–744.

Milne GA and Peros M (2013) Data-model comparison of Holocene sea-level change in the circum-Caribbean region. *Global and Planetary Change* 107: 119–131.

Miyaji N, Ooi N, Noshiro S et al. (2000) Formation process and vegetation history of the Bibai Peatland, central Hokkaido, Japan, during the Holocene. *Japanese Journal of Historical Botany* 8: 15–31 (in Japanese with English abstract).

Morozova GS and Smith ND (1999) Holocene avulsion history of the lower Saskatchewan fluvial system, Cumberland Marshes, Saskatchewan-Manitoba. In: Smith ND and Rogers J (eds) *Fluvial sedimentology VI. Special Publication of International Association of Sedimentologists* 28: 231–249.

Nakada M, Yonekura N and Lambeck K (1991) Late Pleistocene and Holocene sea-level changes in Japan: implications for tectonic histories and mantle rheology. *Palaeogeography, Palaeoclimatology, Palaeoecology* 85: 107–122.

Nijhuis AG, Edmonds DA, Caldwell RL et al. (2015) Fluvio-deltaic avulsions during relative sea-level fall. *Geology* 43: 719–722.

Okuno J, Nakada M, Ishii M et al. (2014) Vertical tectonic crustal movements along the Japanese coastlines inferred from late Quaternary and recent relative sea-level changes. *Quaternary Science Reviews* 91: 42–61.

Ohira A (1995) Holocene evolution of peatland and paleoenvironmental changes in the Sarobetsu Lowland, Hokkaido, northern Japan. *Geographical Review of Japan* 68A: 695–712 (in Japanese

with English abstract).

Ohira A and Umitsu M (1999) Holocene relative sea-level changes and geomorphic development in the riverine-coastal plain around Lake Ohnuma, northern Hokkaido, Japan. *Geographical Review of Japan* 72A: 836–555 (in Japanese with English abstract).

Ono E (2004) Factors affecting late Holocene marine regression in the Nobi Plain, central Japan. *Geographical Review of Japan* 77: 77–98 (in Japanese with English abstract).

Ota Y, Umitsu M and Matsushima Y (1990) Recent Japanese Research on relative sea- level changes in the Holocene and related problems ―Review of studies between 1980 and 1988―. *The Quaternary Research (Daiyonki Kenkyuu)* 29: 31–48 (in Japanese with English abstract).

Peltier WR (2002) On eustatic sea-level histoty: Last Glacial Maximum to Holocene. *Quaternary Science Reviews* 21: 377–396.

Peltier WR (2004) Global glacial isostasy and the surface of the ice-age Earth: the ICE-5G (VM) model and GRACE. *Annual Review of Earth and Planetary Sciences* 32: 111–149.

Reimer PJ, Bard E, Bayliss A et al. (2013) IntCal13 and Marine13 radiocarbon age calibration curves 0-50,000 years cal BP. *Radiocarbon* 55: 1869–1887.

Sagayama T, Tonosaki T, Kondo T et al. (2010) Stratigraphy and paleoenvironment of Upper Pleistocene to Holoecne sediments in the Ishikari Plain, Hokkaido, Japan. *Journal of the Geological Society of Japan* 116: 13–26 (in Japanese with English abstract).

Sakaguchi Y (1974) *Deitanchi no chigaku (Geography of peatland).* Tokyo: University of Tokyo Press (in Japanese).

Sakaguchi Y (1981) Climatic changes of northern Japan during the Holocene epoch. *Geographical Review of Japan* 34: 259–268 (in Japanese with English abstract).

Sakaguchi Y (1993) *Kako 8000 nen no kikouhenka to ningen no rekishi (Climate change and human history during the past 8000 years).* Journal of the Senshu University Research Society 51: 79–113

(in Japanese).

Sato H (2008) Reconstruction of Holocene sea-level change along the coast of Harimanada in the eastern part of the Seto Inland Sea, western Japan. *The Quaternary Research (Daiyonki Kenkyuu)* 47: 247–259 (in Japanese with English abstract).

Segawa A, Minato T and Yoshikawa K (2008) The history of flood plain development and the levee construction of the Ishikari River down stream. *Journal of Construction Management* 15: 429–440 (in Japanese with English abstract).

Shen Z, Törnqvist TE, Mauz B et al. (2015) Episodic overbank deposition as a dominant mechanism of floodplain and delta-plain aggradation. *Geology* 43: 875–878.

Shiga K (2003) Formation of Momijiyama Dune, Ishikari Lowland and changes of diatom assemblages. In: Abstracts of the 110th Annual Meeting of Geological Society of Japan, pp.310.

Slingerland R and Smith ND (2004) River avulsions and their deposits. *Annual Review of Earth and Planetary Sciences* 32: 257–285.

Tada F, Oya M, Sakaguchi Y et al. (1961) The relationship between the flood and topography in the Ishikari River basin. *Report for the Resources Bureau* No. 37. Science and Technology Agency, Japan (in Japanese with English abstract).

Tanabe S, Hori K, Saito Y et al. (2003) Song Hong (Red River) delta evolution related to millennium-scale Holocene sea-level changes. *Quaternary Science Reviews* 22: 2345–2361.

Tanabe S and Ishihara Y (2013) Evolution of the Uppermost Alluvium in the Tokyo and Nakagawa Lowlands, Kanto Plain, central Japan: response to the "Yayoi regression". *The Journal of the Geological Society of Japan* 119: 350–367 (in Japanese with English abstract).

Tanabe S, Hori K, Momohara A et al. (2016) Verification of the "Yayoi regression" in the Tonegawa Lowland, central Japan. *The Journal of the Geological Society of Japan*, submitted (in Japanese with English abstract).

Uehara S and Takeda H (1982) Showa 56 nen 8 gatsu 3 nichi kara 6 nichi ni kaketeno zensen to taihu 12 gou ni yoru Ishikarigawa kouzui saigai oyobi hidaka chihou dosya saigai houkoku (Research report on the flood of Ishikari River and landslide disasters in the Hidaka region due to precipitation front and typhoon No. 12 during 3–6 August 1981). Natural Disaster Research Report No.18 (in Japanese).

Van Asselen S, Stouthamer E and Smith ND (2010) Factors controlling peat compaction in alluvial floodplains: a case study in the cold-temperate Cumberland Marshes, Canada. *Journal of Sedimentary Research* 80: 155–166.

Woodroffe SA, Long AJ, Milne GA et al. (2015) New constraints on late Holocene eustatic sea-level changes from Mahé, Seychelles. *Quaternary Science Reviews* 115: 1–16.

Wright VP and Marriott SB (1993) The sequence stratigraphy of fluvial depositional systems: the role of floodplain sediment storage. *Sedimentary Geology* 86: 203–210.

Wüst RAJ, Bustin RM and Lavkulich LM (2003) New classification systems for tropical organic-rich deposits based on studies of the Tasek Bera Basin, Malaysia. *Catena* 53: 133–163.

Xu Q, Xiao J, Li Y et al. (2010) Pollen-based quantitative reconstruction of Holocene climate changes in the Daihai Lake area, Inner Mongolia, China. *Journal of Climate* 23: 2856–2868.

Yokoyama Y, Nakada M, Maeda Y et al. (1996) Holocene sea-level change and hydro-isostasy along the west coast of Kyushu, Japan. *Palaeogeography, Palaeoclimatology, Palaeoecology* 123: 29–47.

Yokoyama Y, Okuno J, Miyairi Y et al. (2012) Holocene sea-level change and Antarctic melting history derivedf from geological observations and geophysical modeling along the Shimokita Peninsula, northern Japan. *Geophysical Research Letters* 39: L13502.

Yokoyama Y, Maeda Y, Okuno J et al. (2015) Holocene Antarctic melting and lithospheric uplift history of the southern Okinawa trough inferred from mid- to late-Holocene sea level in Iriomote Island, Ryukyu, Japan. *Quaternary International*, in press.

Captions of figures:

Figure 1. Map showing the study area. (a) Location of the Ishikari lowland. (b) Shaded relief map showing location of the landform classification map of Figure 2.

Figure 2. Landform classification map of the study area (after Ishii et al., 2014). Locations of cores and basal ages of the Uppermost Peat are also shown.

Figure 3. Annual maximum discharges and corresponding water levels of the Ishikari River between 1975 and 2012 at Tsukigata. The water levels are relative to the mean sea level.

Figure 4. Sedimentary logs and LOI data for selected cores. Dashed line indicates the base of the Uppermost Peat. Core P43 was obtained several meters from core P16 site for detailed plant macrofossil analysis, and its sedimentary column essentially duplicates that of P16.

Figure 5. Age-altitude plot, sedimentary column, and physical data of core IK1. (a) Sedimentation rate curve based on ^{14}C dating. (b) Sedimentary log of core IK1. (c) Bulk density, water content, LOI, and grain size data for core IK1. Dashed line indicates the base of the Uppermost Peat.

Figure 6. Plant macrofossil and LOI data from cores.

Figure 7. Relationship between clastic sedimentation rate and LOI. Solid curves show the theoretical relationship between clastic sedimentation rate and LOI, calculated using equations (3)–(5) and three different values of organic sedimentation rate. The grey areas show the errors arising from the uncertainty of the ρ_{peat}. The depth intervals depend on the ^{14}C ages obtained in core IK1. White

symbols represent core depths predominantly consisting of peat, black symbols represent core depths that include thin peat beds as well as overbank deposits, and gray symbols represent core depths without peat. Clastic sedimentation rates between 7.4 and 9.3 m were greater than 3 mm/yr and are omitted from the graph.

Figure 8. Ages of peat initiation and comparison with paleoclimate proxy records. (a) Age–altitude plots and (b) probability density of ^{14}C ages obtained within 0.3 m and 0.1 m of the base of the Uppermost Peat. (c) Proxy record of EASM ($\delta^{18}O$ of stalagmite D4, Dongge Cave, China, Dykoski et al., 2005). (d) Eustatic sea-level model (Bradley et al., 2011).

Table 1. Summary of radiocarbon dates in cores.

Table 2. Estimated initiation ages of the Uppermost Peat. Sedimentation rates were calculated using the depths and the median probability of ^{14}C ages.

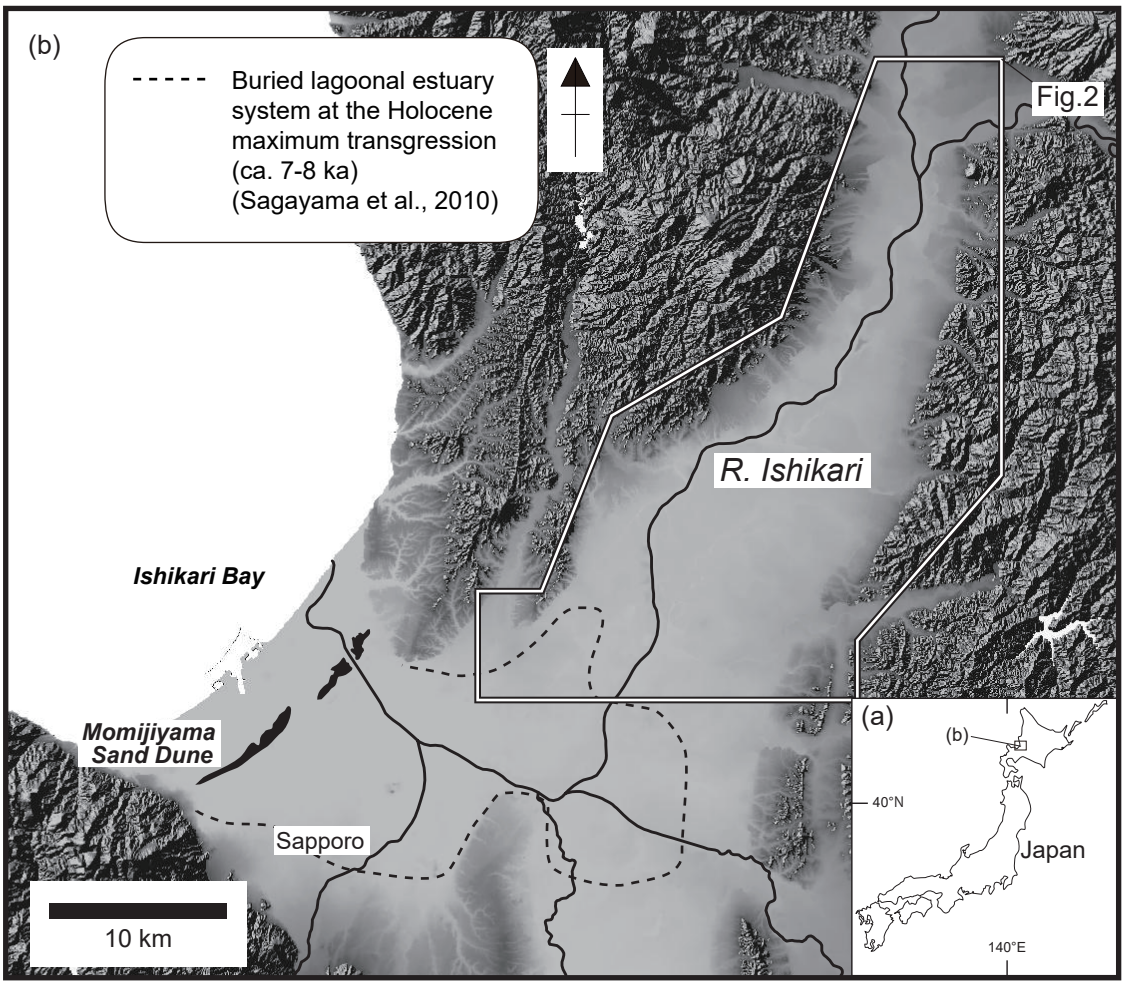
(b)
Buried lagoonal estuary system at the Holocene maximum transgression (ca. 7-8 ka) (Sagayama et al., 2010)
Fig.2
R. Ishikari
Ishikari Bay
Momijiyama Sand Dune
Sapporo
10 km
(a)
(b)
40°N
Japan
140°E

Figure 1

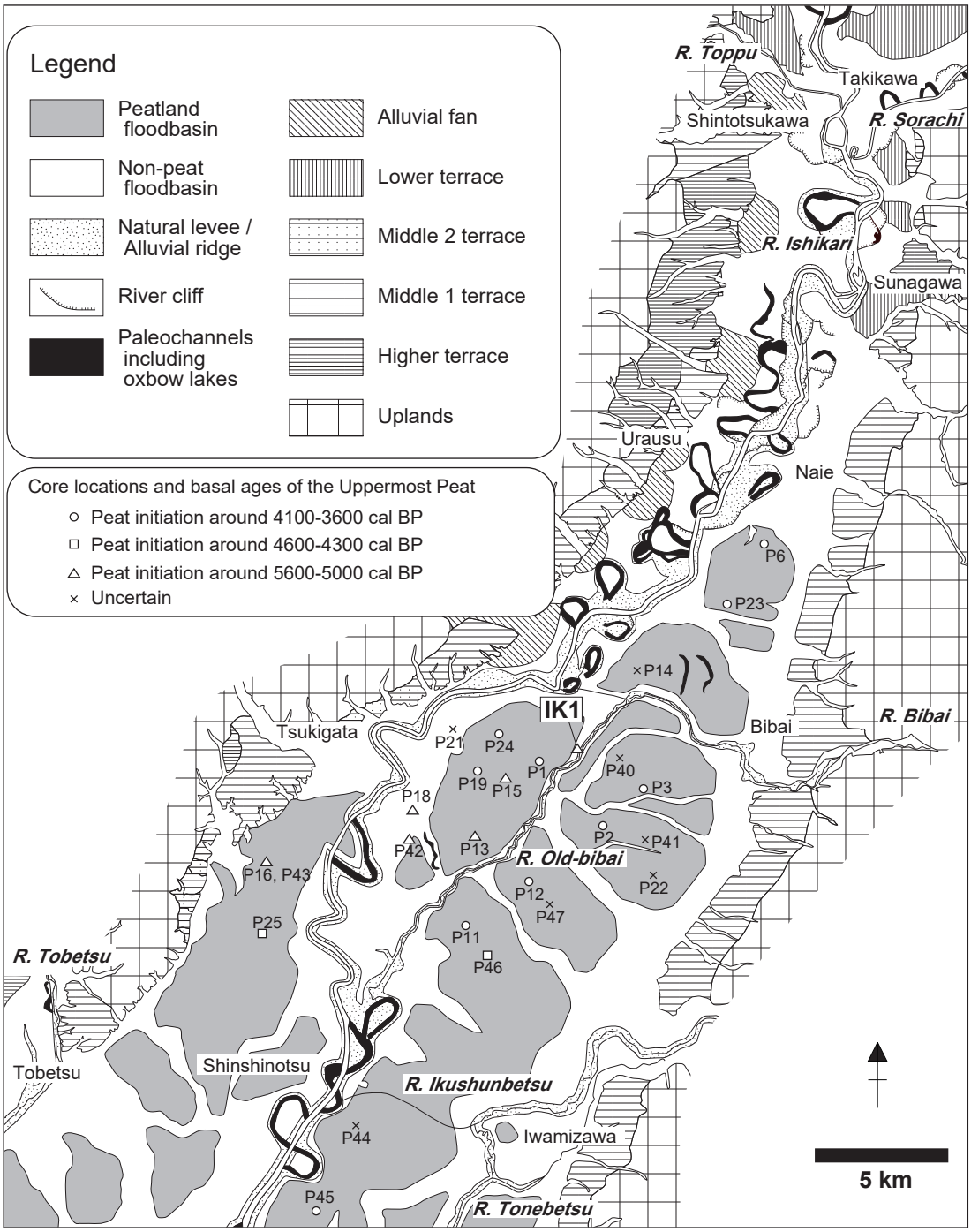
Legend
Peatland floodbasin
Non-peat floodbasin
Natural levee / Alluvial ridge
River cliff
Paleochannels including oxbow lakes
Alluvial fan
Lower terrace
Middle 2 terrace
Middle 1 terrace
Higher terrace
Uplands
Core locations and basal ages of the Uppermost Peat
Peat initiation around 4100-3600 cal BP
Peat initiation around 4600-4300 cal BP
Peat initiation around 5600-5000 cal BP
Uncertain
R. Toppu
Takikawa
Shintotsukawa
R. Sorachi
R. Ishikari
Sunagawa
Urausu
Naie
P6
P23
P14
IK1
Tsukigata
Bibai
R. Bibai
P21
P24
P1
P40
P19
P15
P3
P18
P2
P41
P42
P13
R. Old-bibai
P16, P43
P22
P12
P47
P25
P11
P46
R. Tobetsu
Tobetsu
Shinshinotsu
R. Ikushunbetsu
P44
Iwamizawa
P45
R. Tonebetsu
5 km

Figure 2

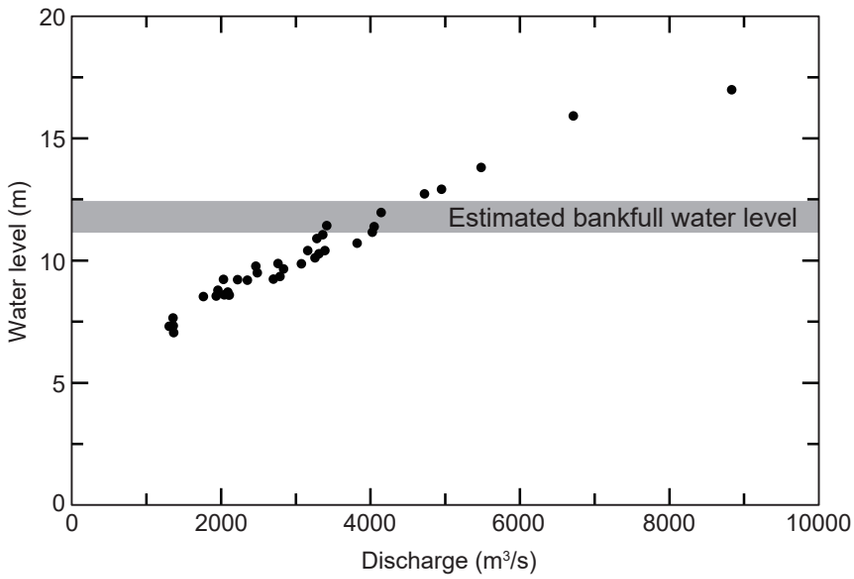
Water level (m)
Discharge (m³/s)
Estimated bankfull water level
0
5
10
15
20
0
2000
4000
6000
8000
10000

Figure 3

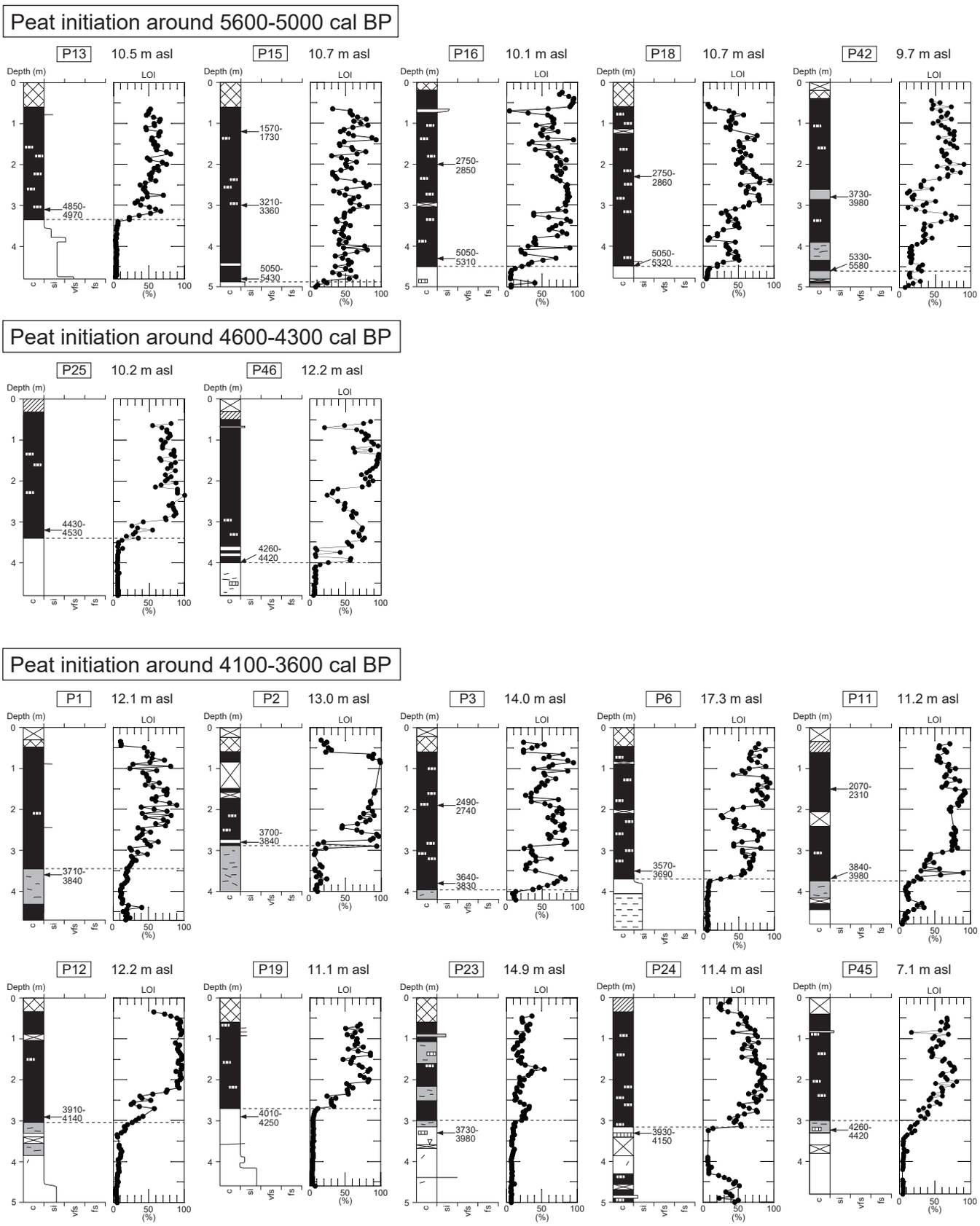
Peat initiation around 5600-5000 cal BP
P13 10.5 m asl
4850-4970
P15 10.7 m asl
1570-1730
3210-3360
5050-5430
P16 10.1 m asl
2750-2850
5050-5310
P18 10.7 m asl
2750-2860
5050-5320
P42 9.7 m asl
3730-3980
5330-5580
Peat initiation around 4600-4300 cal BP
P25 10.2 m asl
4430-4530
P46 12.2 m asl
4260-4420
Peat initiation around 4100-3600 cal BP
P1 12.1 m asl
3710-3840
P2 13.0 m asl
3700-3840
P3 14.0 m asl
2490-2740
3640-3830
P6 17.3 m asl
3570-3690
P11 11.2 m asl
2070-2310
3840-3980
P12 12.2 m asl
3910-4140
P19 11.1 m asl
4010-4250
P23 14.9 m asl
3730-3980
P24 11.4 m asl
3930-4150
P45 7.1 m asl
4260-4420
Depth (m)
LOI
c
si
vfs
fs
(%)

Figure 4

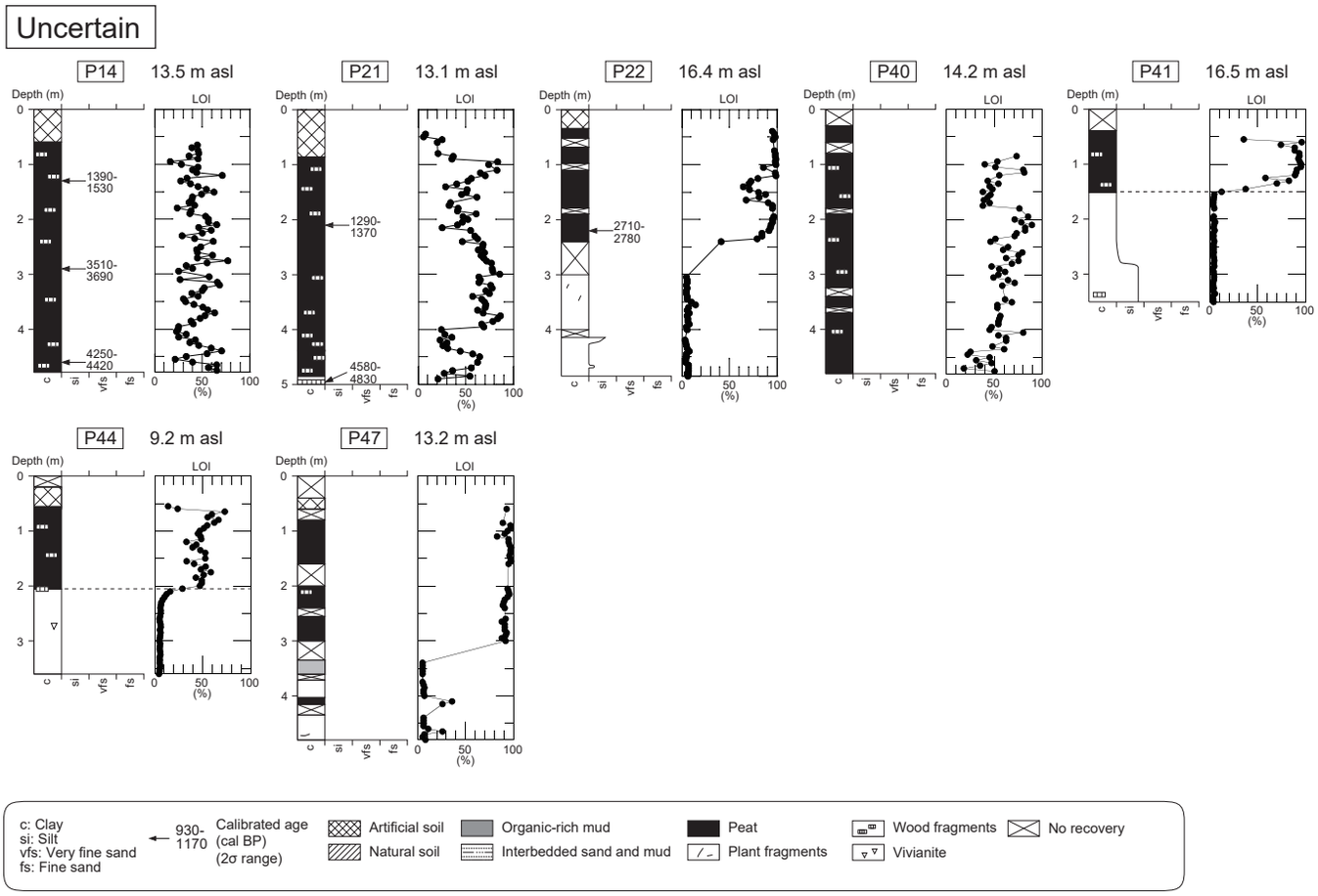

Figure 4 (continued)

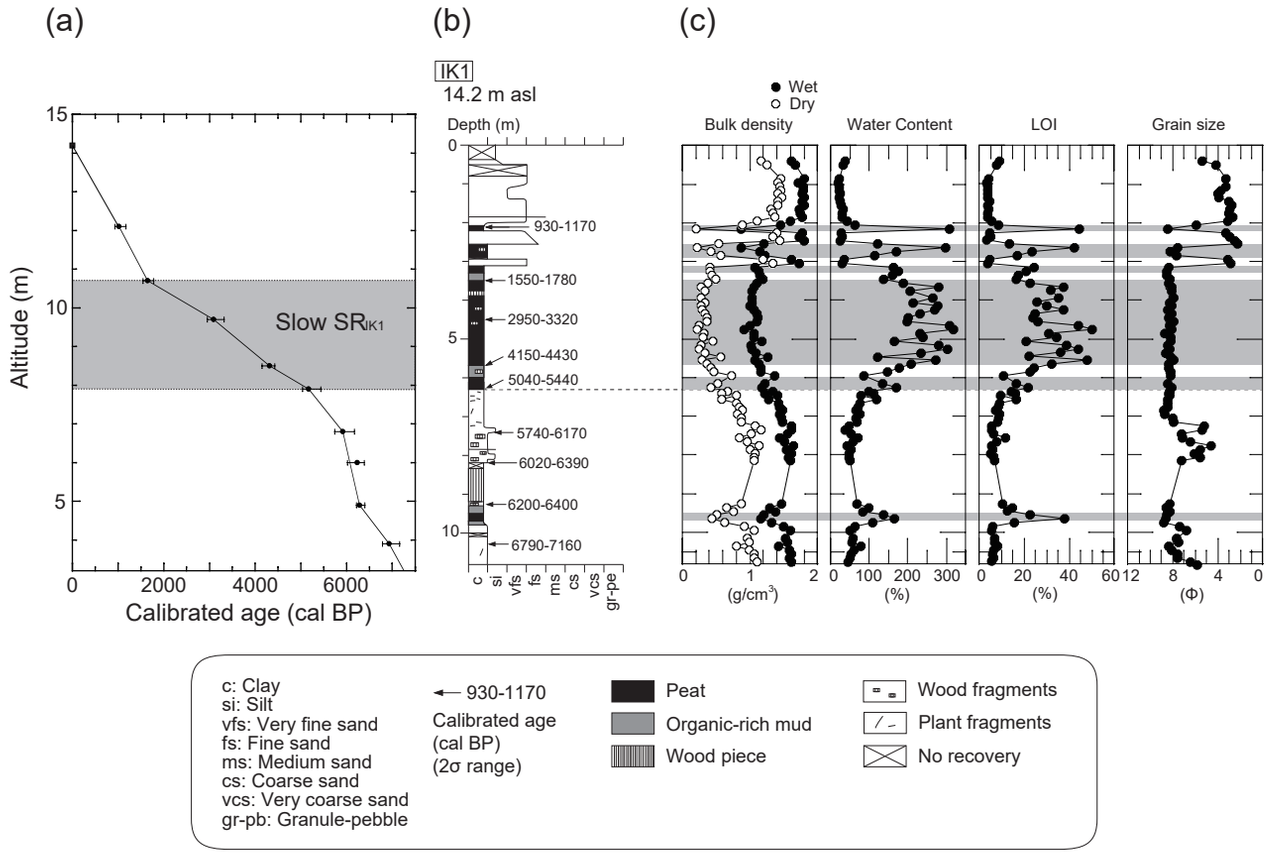
(a)
(b)
(c)
Altitude (m)
Calibrated age (cal BP)
Slow SRIK1
IK1
14.2 m asl
Depth (m)
930-1170
1550-1780
2950-3320
4150-4430
5040-5440
5740-6170
6020-6390
6200-6400
6790-7160
c
si
vfs
fs
ms
cs
vcs
gr-pe
Wet
Dry
Bulk density
Water Content
LOI
Grain size
(g/cm3)
(%)
(%)
(Φ)
c: Clay
si: Silt
vfs: Very fine sand
fs: Fine sand
ms: Medium sand
cs: Coarse sand
vcs: Very coarse sand
gr-pb: Granule-pebble
930-1170
Calibrated age
(cal BP)
(2σ range)
Peat
Organic-rich mud
Wood piece
Wood fragments
Plant fragments
No recovery

Figure 5

(a)

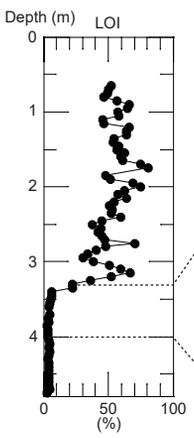

P13

Depth (cm)	*Carex* spp. A type (fruit)	LOI (%)
325-330	5	22.3
330-335	1	22.3
335-340	-	6.4
340-345	1	5.9
345-350	-	5.3
350-355	-	4.5
355-360	-	4.2
380-385	-	3.0
385-390	-	3.4
395-400	-	4.0

(b)

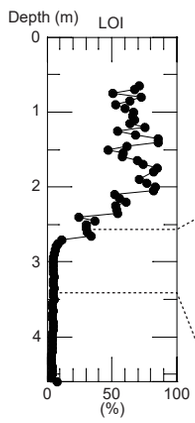

P19

Depth (cm)	*Carex* spp. A type (fruit)	LOI (%)
255-260	1	30.9
260-265	2	33.7
265-270	4	10.9
270-275	-	8.2
275-280	-	6.8
280-285	-	5.9
285-290	-	5.1
290-295	-	4.7
295-300	-	4.7
305-310	-	4.8
315-320	-	5.2
335-340	-	4.8

(c)

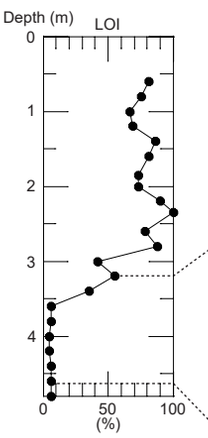

P25

Depth (cm)	*Carex* spp. A type (fruit)	*Carex* sect. *Stellulatae* (fruit)	*Carex* sect. *Phacocystis* (fruit)	*Menyanthes trifoliata* (seed)	LOI (%)
315-320	1	-	-	-	55.4
335-340	10	-	-	-	35.1
345-350	-	-	-	-	-
355-360	-	-	-	-	6.1
375-380	-	-	-	-	5.6
385-390	-	-	-	-	-
395-400	-	-	-	1	5.4
415-420	-	-	-	-	4.8
435-440	-	1	-	-	6.0
455-460	-	-	1	-	5.7

(d)

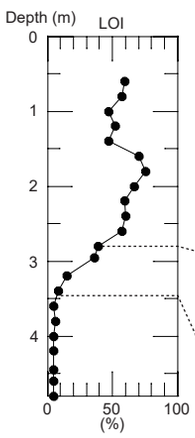

P45

Depth (cm)	*Carex* spp. A type (fruit)	*Carex* sect. *Stellulatae* (fruit)	*Carex* sect. *Phacocystis* (fruit)	*Achillea* sp. (fruit)	*Menyanthes trifoliata* (seed)	*Ampelopsis brevipedunculata* (seed)	LOI (%)
275-280	1	-	1	-	-	-	39.2
305-310	-	1	1	-	-	-	-
310-315	-	-	-	-	-	-	-
315-320	-	-	-	1	-	1	14.6
325-330	-	-	-	-	1	-	-
330-335	-	-	-	-	-	-	-
335-340	-	-	-	-	-	-	8.4
340-345	-	-	-	-	-	-	-

(e)

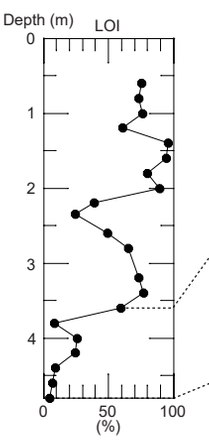

P46

Depth (cm)	*Carex* spp. A type (fruit)	*Triadenum japonicum* (seed)	*Eriocaulon* sp. (seed)	LOI (%)
355-360	3	-	-	59.0
375-380	-	-	-	7.7
395-400	4	5	-	25.9
415-420	5	-	-	-
435-440	1	-	-	8.6
455-460	-	-	1	6.6
475-480	2	-	-	5.2

(f)

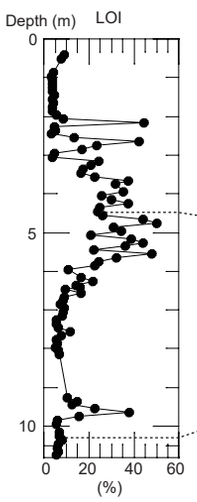

IK1

Depth (cm)	*Carex* spp. A type (fruit)	*Triadenum japonicum* (seed)	*Schoenoplectus* sp. (fruit)	LOI (%)
445-450	-	-	-	-
575-580	-	-	-	-
650-655	4	-	-	16.7
675-680	1	-	-	-
695-700	7	-	-	-
735-740	-	-	-	-
975-980	19	1	-	-
1035-1040	-	-	1	-
1055-1060	-	-	-	-

Figure 6

(g)

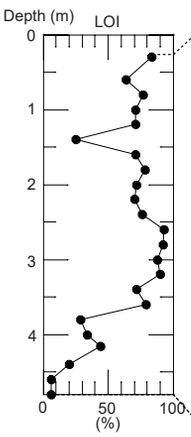

P43

Depth (cm)	*Carex* spp. A type (fruit)	*Carex* sect. *Stellulatae* (fruit)	*Carex* sect. *Phacocystis* (fruit)	*Carex* spp. (utricle)	*Schoenoplectus* sp. (fruit)	*Rhynchospora* sp. (fruit)	*Eriocaulon* sp. (seed)	*Triadenum japonicum* (seed)	*Lycopus* sp. (fruit)	Poaceae (caryopsis)	*Polygonum thunbergii* (fruit)	*Viola* sp. (seed)	*Lobelia sessilifolia* (seed)	*Potamogeton* sp. (fruit)	*Menyanthes trifoliata* (seed)	*Alnus japonica* (fruit)	*Myrica gale* (seed)	LOI (%)
25-30	-	-	-	-	-	-	-	-	-	-	-	-	-	-	-	-	6	82.8
55-60	-	-	-	-	-	-	-	-	-	-	-	-	-	-	-	-	-	63.9
75-80	-	1	-	-	-	-	-	-	-	-	-	-	-	-	-	-	-	77.0
95-100	-	-	-	-	-	1	-	-	-	-	-	-	-	-	-	-	-	70.6
115-120	-	-	-	-	-	-	-	-	7	-	-	-	-	-	-	-	-	70.6
135-140	1	-	1	-	-	-	-	-	-	2	-	-	-	-	-	-	-	25.2
135-160	-	-	-	-	-	-	-	-	-	-	-	-	-	-	-	-	-	70.9
175-180	-	1	-	-	-	1	-	1	-	-	-	-	-	-	-	-	-	77.7
195-200	-	-	-	-	-	-	-	-	-	-	-	-	-	-	-	-	-	71.6
215-220	-	-	-	-	-	10	1	1	-	-	-	1	-	-	-	-	-	69.5
235-240	-	-	-	-	-	2	-	-	-	-	-	-	1	-	2	-	-	76.5
255-260	-	-	-	-	-	1	-	-	-	-	-	-	-	-	1	-	-	93.0
275-280	-	-	-	1	-	-	-	-	-	-	-	-	-	-	-	-	-	92.2
295-300	3	2	-	-	-	-	-	-	1	-	-	-	-	-	-	-	-	88.4
315-320	-	1	-	-	-	-	1	1	-	-	-	2	-	-	-	-	-	89.7
335-340	-	-	-	-	-	-	-	1	-	-	-	-	-	-	-	-	2	72.3
355-360	1	-	-	1	-	-	-	-	-	-	-	-	-	-	-	-	-	78.8
375-380	-	-	-	1	-	-	-	-	-	-	-	-	-	-	-	-	-	28.7
395-400	-	-	-	-	-	-	-	-	-	-	1	-	-	-	-	-	-	34.1
410-415	3	-	-	-	-	-	-	-	-	-	-	-	-	-	-	1	-	44.4
425-430	1	-	-	1	-	-	-	4	-	-	-	-	-	-	-	-	-	-
430-435	5	2	-	-	-	-	-	6	-	-	-	-	-	-	-	-	-	-
435-440	1	-	-	-	14	-	-	-	-	-	-	-	-	-	-	-	-	19.7
445-450	-	-	-	-	5	-	-	-	-	-	-	-	-	1	-	-	-	-
455-460	-	-	-	-	-	-	-	-	-	-	-	-	-	-	-	-	-	6.4
465-470	-	-	-	-	-	-	-	-	-	-	-	-	-	-	-	-	-	-
470-475	-	-	-	-	-	-	-	-	-	-	-	-	-	-	-	-	-	-
478-480	-	-	-	-	-	-	-	-	-	-	-	-	-	1	-	-	-	6.4

Figure 6 (continued)

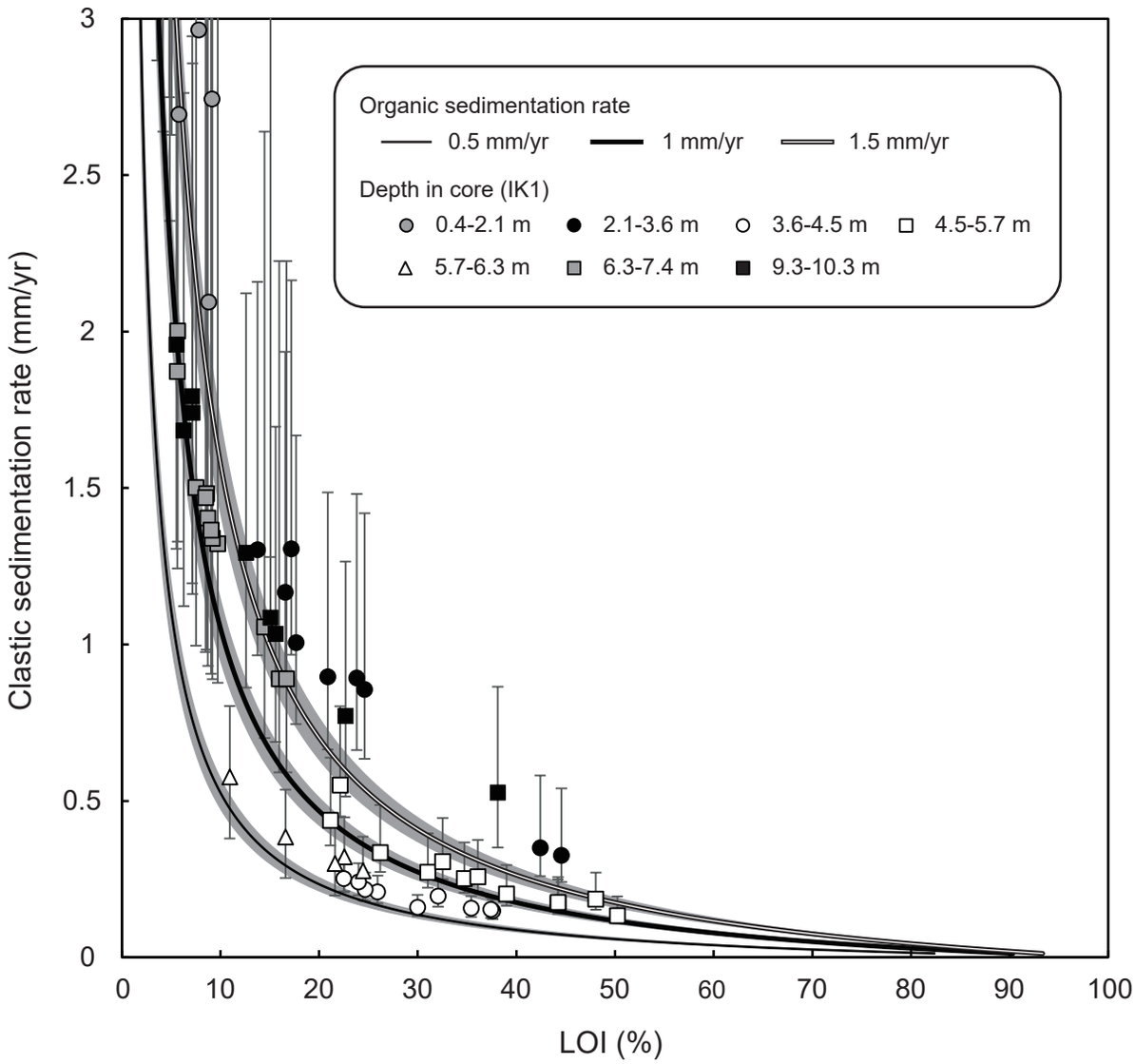
Organic sedimentation rate
0.5 mm/yr
1 mm/yr
1.5 mm/yr
Depth in core (IK1)
0.4-2.1 m
2.1-3.6 m
3.6-4.5 m
4.5-5.7 m
5.7-6.3 m
6.3-7.4 m
9.3-10.3 m
Clastic sedimentation rate (mm/yr)
LOI (%)
0
0.5
1
1.5
2
2.5
3
0
10
20
30
40
50
60
70
80
90
100

Figure 7

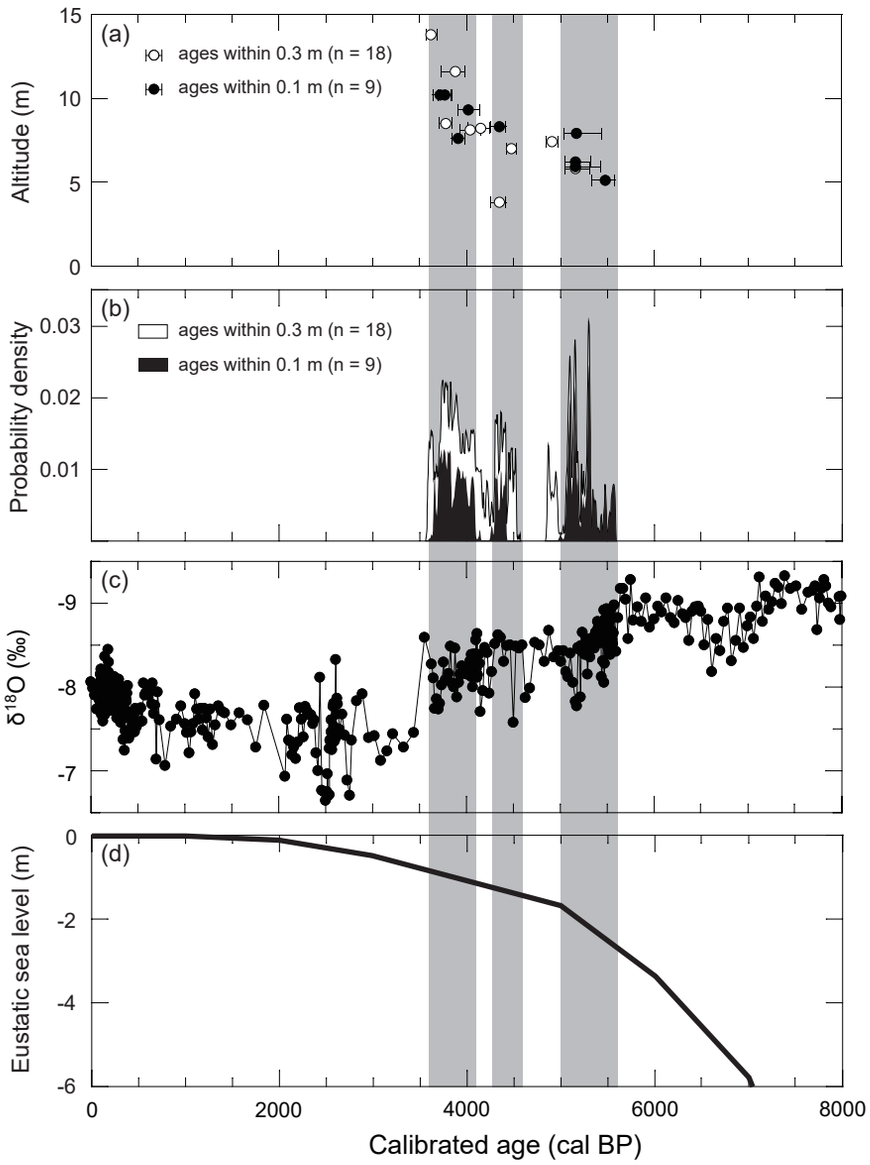
(a)
ages within 0.3 m (n = 18)
ages within 0.1 m (n = 9)
Altitude (m)
15
10
5
0
(b)
ages within 0.3 m (n = 18)
ages within 0.1 m (n = 9)
Probability density
0.03
0.02
0.01
(c)
δ18O (‰)
-9
-8
-7
(d)
Eustatic sea level (m)
0
-2
-4
-6
0
2000
4000
6000
8000
Calibrated age (cal BP)

Figure 8

Sample code	Depth (m)	Altitude (m)	Dated material	^{14}C age (yrs BP)	Error (1σ)	Calibrated age (cal BP) (2σ range)	Median probability (cal BP)	Laboratory code
IK1-2-210	2.1	12.1	Wood piece	1110	40	930-1170	1020	KGM-OWd110067*
IK1-4-350	3.5	10.7	Wood piece	1740	40	1550-1780	1650	KGM-OWd110068*
IK1-6-452	4.5	9.7	Wood piece	2940	50	2950-3320	3090	KGM-OWd110069*
IK1-7-573	5.7	8.5	Wood piece	3890	50	4150-4430	4320	KGM-OWd110070*
IK1-8-627	6.3	7.9	Wood piece	4540	50	5040-5440	5170	KGM-OWd110071*
IK1-10-740	7.4	6.8	Wood piece	5160	60	5740-6170	5920	KGM-OWd110072*
IK1-10-820	8.2	6	Wood piece	5440	50	6020-6390	6240	KGM-OWd110073*
IK1-12-925	9.3	4.9	Wood piece	5490	50	6200-6400	6290	KGM-OWd110074*
IK1-13-1028	10.3	3.9	Plant fragments	6070	60	6790-7160	6930	KGM-OWd110075*
pf1-360/365-1	3.6	8.5	Plant fragments	3510	20	3710-3840	3780	UCIAMS-120181
pf2-280/285-3	2.8	10.2	Plant fragments	3500	20	3700-3840	3770	UCIAMS-120179
pf3-375/380-8	3.8	10.2	Plant fragments	3450	30	3640-3830	3720	UCIAMS-120180
pf6-350/355-2	3.5	13.8	Plant fragments	3375	20	3570-3690	3620	UCIAMS-120183
3-190	1.9	12.1	Plant fragments	2515	30	2490-2740	2590	D-AMS-005444
11-150	1.5	9.7	Wood piece	2175	30	2070-2310	2230	D-AMS-005445
11-360	3.6	7.6	Wood piece	3600	30	3840-3980	3910	D-AMS-005446
12-290	2.9	9.3	Twig	3680	30	3910-4140	4020	D-AMS-005447
13-310	3.1	7.4	Wood piece	4340	30	4850-4970	4910	D-AMS-005448
14-130	1.3	12.2	Plant fragments	1570	30	1390-1530	1470	D-AMS-005449
14-350	3.5	10	Wood piece	3365	30	3510-3690	3610	D-AMS-005450
14-460	4.6	8.9	Twig	3900	30	4250-4420	4340	D-AMS-005451
15-120	1.2	9.5	Wood piece	1750	30	1570-1730	1660	D-AMS-005452
15-270	2.7	8	Wood piece	3065	30	3210-3360	3280	D-AMS-005453
15-480	4.8	5.9	Wood piece	4555	35	5050-5430	5160	D-AMS-005454
16-200	2	8.1	Wood piece	2690	30	2750-2850	2790	D-AMS-005455
16-430	4.3	5.8	Wood piece	4535	35	5050-5310	5160	D-AMS-005456
18-230	2.3	8.4	Wood piece	2700	35	2750-2860	2800	D-AMS-005457
18-450	4.5	6.2	Wood piece	4550	30	5050-5320	5160	D-AMS-005458
19-290	2.9	8.2	Twig	3780	30	4010-4250	4150	D-AMS-005459
21-210	2.1	11	Twig	1415	30	1290-1370	1320	D-AMS-005460
22-220	2.2	14.2	Wood piece	2600	30	2710-2780	2740	D-AMS-005461
21-500	5	8.1	Wood piece	4165	30	4580-4830	4710	D-AMS-005462
23-330	3.3	11.6	Wood piece	3575	30	3730-3980	3880	D-AMS-005463
P25-320	3.2	7	Twig	4020	20	4430-4530	4480	PLD-27619
P42-460	4.6	5.1	Twig	4730	30	5330-5580	5480	PLD-27624
P45-325	3.3	3.8	Wood piece	3900	20	4260-4420	4350	PLD-27625
P46-390	3.9	8.3	Wood piece	3910	20	4260-4420	4350	PLD-27626
P24-330	3.3	8.1	Wood piece	3700	35	3930-4150	4040	D-AMS-009110
P42-260	2.6	7.1	Wood piece	3585	35	3730-3980	3890	D-AMS-009117

* After Ishii et al. (2014)

Table 1

Location	Depth of ^{14}C age (m)	Calibrated age (cal BP) (2σ range)	Median probability (cal BP)	Sedimentation rate (mm/yr)	Basal depth of Uppermost Peat (m)	Estimated age of onset of Uppermost Peat (cal BP)	Depth difference between ^{14}C age and base of the Uppermost Peat (m)
P13	3.1	4850-4970	4910	0.6	3.4	5100	0.3
P15	4.8	5050-5430	5160	0.9	4.9	5250	0.1
P16	4.3	5050-5310	5160	0.8	4.5	5330	0.2
P18	4.5	5050-5320	5160	0.9	4.5	5160	< 0.1
P42	4.6	5330-5580	5480	0.8	4.6	5480	< 0.1
IK1	6.3	5040-5440	5170	1.2	6.3	5170	< 0.1
P25	3.2	4430-4530	4480	0.7	3.4	4620	0.2
P46	3.9	4260-4420	4350	0.9	4.0	4440	0.1
P1	3.6	3710-3840	3780	1.0	3.4	3590	0.2
P2	2.8	3700-3840	3770	0.7	2.9	3840	0.1
P3	3.8	3640-3830	3720	1.0	3.9	3820	0.1
P6	3.5	3570-3690	3620	1.0	3.7	3810	0.2
P11	3.6	3840-3980	3910	0.9	3.7	4000	0.1
P12	2.9	3910-4140	4020	0.7	3.0	4090	0.1
P19	2.9	4010-4250	4150	0.7	2.6	3940	0.3
P23	3.3	3730-3980	3880	0.9	3	3620	0.3
P24	3.3	3930-4150	4040	0.8	3.1	3880	0.2
P45	3.3	4260-4420	4350	0.8	3.0	4120	0.3

Table 2